UNIVERSITY OF BIRMINGHAM

Research at Birmingham

DEM-CFD analysis of contact electrification and electrostatic interactions during fluidization

Pei, Chunlei; Wu, Chuan-yu; Adams, Michael

Link to publication on Research at Birmingham portal

Accepted Manuscript

DEM-CFD analysis of contact electrification and electrostatic interactions during fluidization

Chunlei Pei, Chuan-Yu Wu, Michael Adams

Please cite this article as: Chunlei Pei, Chuan-Yu Wu, Michael Adams, DEM-CFD analysis of contact electrification and electrostatic interactions during fluidization, *Powder Technology* (2016), doi: 10.1016/j.powtec.2016.08.030

DEM-CFD analysis of contact electrification and electrostatic interactions during fluidization

Chunlei Pei[1&], Chuan-Yu Wu[1*] and Michael Adams[2]

[1] Department of Chemical and Process Engineering, University of Surrey, Guildford, GU2 7XH, UK

[2] School of Chemical Engineering, University of Birmingham, Birmingham, B15 2TT, UK

Abstract

Contact electrification and electrostatic interactions often occur in the fluidization process, which can significantly influence the dynamic behaviour of particles and the fluidization performance. In this study, a discrete element method coupled with computational fluid dynamics (DEM-CFD) is developed by implementing contact electrification and electrostatic interaction models and the combined effects of contact electrification and electrostatic interaction on fluidization are analysed. It is found that the charge of the particle system increase with the superficial gas velocity. Particles of different material properties (especially work function) can be bi-charged and form agglomerates. At low superficial gas velocities, the particle bed cannot be fully fluidized and the pressure drop tends to be stable rather than fluctuating as the gas flows through the micro-channels of agglomerates. However, at high superficial gas velocities, the agglomerates can break, inducing strong fluctuation of pressure drop. Clearly, the electrostatic phenomena and fluidization behaviour can mutually influence each other during the process.

[&] Presently with Department of Materials Science and Metallurgy, University of Cambridge, Cambridge, CB3 0FS, UK

[*] Corresponding author: Tel: 01483683506; Email: c.y.wu@surrey.ac.uk

1. Introduction

In gas-solid fluidisation, contact electrification and electrostatic interactions between particles are common phenomena [1]. Contact electrification is referred to as the charge transfer process between objects (particle-particle & particle-wall) during collisions. Once the net charge transferred onto particles are strong enough, the induced repulsive and attractive electrostatic forces between objects can cause agglomeration [2,3], dispersion [4] and segregation [5], which will significantly affect the dynamic behaviours of particles and the performance of the fluidisation process.

The fluidisation process involves intensive interactions between particles and the fluid, specifically gas in gas-solid fluidisation. The frequent collisions and intensive mixing of particles could result in effective contact electrification and consequent electrostatic interactions [6–10]. Guardiola et al. [6] investigated electrification during fluidization using glass beads of various sizes at different fluidization velocities and relative humidity. The potential difference, as the degree of electrification, between the granular bed and the earthed distributor could reach a constant value under various conditions as the fluidizing process continues. They found that the degree of electrification increased with increasing fluidization velocity at a relatively lower humidity, which was attributed to the facts that a higher gas velocity facilitated the motion of the particles in the fluidized bed, leading to more collisions between particles, while the lower humidity inhibited the charge dissipation. Wolny and Kaźmierczak [7,8] showed experimentally that polymer particles could acquire both positive and negative charge and form agglomerates during fluidisation. As a result, micro-channels were developed and led to smaller pressure drops but higher minimum bubbling velocities.

Non-Newtonian fluid behaviours was observed in the fluidised bed with strong electrostatic interactions, especially at lower superficial gas velocities (closer to the minimum bubbling velocity). In addition, the adhesion of particles onto walls at lower humidity was also observed by Zhang et al. [9], when the particle motion was examined in the gas-solid fluidized bed. Liu et al. [10] investigated the electrostatic changing behaviours of insulating particles in pressurized fluidized bed and suggested that the electrification of particle could be enhanced by increasing the superficial gas velocity. The interplay between electrification and fluidisation makes it difficult to understand the relationship between the hydrodynamic pressure of the fluidised bed and the charging behaviour of particles during the process.

In order to understand dynamic behaviours of particles and fluid, the discrete element method coupled with computational fluid dynamics (DEM-CFD) is extensively employed to model the contact electrification and electrostatic interactions in the fluidisation process [11,12]. For instance, Pei et al. [11] implemented a contact electrification (condenser) model into DEM-CFD and examined charge accumulation and distribution of powders during fluidisation. They showed that the charge accumulated exponentially during fluidisaiton and eventually reached an equilibrium value. The charge originated from the contact between particles and walls and propagated from the region near the wall to the centre of the column. The results were in broad agreement with experimental observations of Guardiola *et al.* [6] and LaMarche et al. [13], although electrostatic interactions were not considered in the simulations. Hassani et al. [12] investigated the bubble hydrodynamics of the fluidisation with neutral and charged particles using DEM-CFD. The charge of particles was assumed to be same and constant. For mono-charged particles, bubbles tended to become smaller and even disappear when the mutual repulsive force was significantly larger than the weight of the particle [4,14]. On the other hand, as the bi-charged particles experienced both repulsive

4

and attractive forces, chain-like clusters of particles were observed in the bubbling regime. In addition, particle segregation and lower mixing efficiency due to the strong electrostatic forces during fluidisation were also observed in the DEM-CFD simulations [15]. However, as the charge of the particles was fixed, the dynamic charging process due to collision was not modelled with electrostatic interactions. Since the charge transfer process and electrostatic interactions are dynamic and concurrent during fluidisation, it is crucial to consider the combined effects of contact electrification and electrostatic interactions on the fluidisation process.

In this study, the DEM-CFD method is further advanced with the implementation of contact electrification and electrostatic interaction models in order to investigate their influences on the fluidisation behaviour. The charge accumulation and distribution during fluidisation are analysed. The performance of the fluidisation at various superficial gas velocities is examined. The interplay between electrostatics and fluidisation conditions is also explored.

2. DEM-CFD modelling

2.1 The contact electrification model

During fluidisation, both the contact electrification process and subsequent electrostatic interactions are dynamic in nature, in which the charge acquisition and transfer are determined by collisions between particles while electrostatic interactions depend on the charge on particles and distance between particles. The contact electrification model in this DEM model is for spherical particles, which is same as the model reported in Pei et al. [11]. When a contact takes place, the charge can be transferred from one surface to another due to the total potential difference that can be expressed as:

$$\Delta V = V_c - V^{'} = V_i - V_j - V^{'} \tag{1}$$

where ΔV is the total potential difference; V_c ($=V_i$ - V_j) is the contact potential difference (CPD) between the surfaces; $V^{'}$ is the induced potential difference; V_i and V_j are the work function potentials of the material i and j, respectively.

The induced potential difference is caused by the electric field between two charged objects [16]. The induced potential between the wall surface and the uniformly charged sphere is given as follows:

$$V^{'} = k_0 q = \xi \frac{z}{\varepsilon_0} A^{-1} q \tag{2}$$

where A is the surface area of the spherical particle; q is the charge of the particle; ε_0 is the permittivity of a vacuum (8.854×10^{-12} F·m^{-1}), z is the contact gap for tunnel relaxation and is generally of the order of a few nano-meters to hundreds of nano-meters [17,18]. It is assumed to be 130 nm in the current study. ξ is the image correction factor for the polarization effect. The induced electric field can further polarize the surface and cause the image effects. If the image effects are considered, the induced potential difference can be affected by the image correction factor, depending on the dielectric properties and the contact gap [16]. In the current study, the wall surface is assumed to be conductive, so this image correction factor is set to 2 [1,16]. It should be noted that, according to Eqs (1) and (2), the CPD will be eventually balanced by the induced potential difference that is determined by the charge of particles and the induced image effects. Therefore, the image correction factor can influence

the final equilibrium charge on the particle. For instance, provided that the CPD is constant, the final equilibrium charge decreases with the increase of the image correction factor. In other words, the dielectric properties and contact conditions can play an important role in the charging transfer process.

If two charged spheres of insulating materials are considered, then the induced potential difference can be determined as:

$$V^{'} = \frac{z}{\varepsilon_0}\left(\frac{q_j}{A_j} - \frac{q_i}{A_i}\right)$$ (3)

where q_i and q_j are the charges of spheres i and j; A_i and A_j are the surface areas of the spheres i and j. In the current study, spherical particles are assumed to be non-polarizable insulators so the charge does not relax and redistribute on spheres. The contact gap between spheres, z is set to 260 nm and the image effects between particles are ignore.

Based on the condenser model [1,11], the CPD ($V_c = V_i - V_j$) is the driving force for electron transfer between contacting surfaces. In each collision, the transferred charge is proportional to the maximum contact area and the total potential difference, i.e.

$$\Delta q = k_s S_m \Delta V$$ (4)

where S_m is the maximum contact area during the collision, k_s is the charging constant during contact electrification and is of the order of 10^{-4} C·m^{-2}·V^{-1} [19–21]. During a collision, the

charge will be transferred from material *i* to material *j*. Hence after each collision, the charge on these materials will become $q_{si}-\Delta q$ and $q_{sj}+\Delta q$, respectively.

2.2 The electrostatic interaction model

The charge on particles can induce electric field, which will lead to electrostatic interactions between charged objects [4]. The electrostatic interaction between point charges is governed by the Coulomb's law. In this study, as a first approximation, the charge is assumed to distribute uniformly on the surface of a spherical particle and cannot be polarized. Then the electrostatic interaction between charged particles is governed by the Coulomb's law as:

$$\mathbf{F}_{ij}^{e} = \frac{1}{4\pi\varepsilon_0} \frac{q_i q_j}{r_{ij}^2} \mathbf{n}_{ij}$$ (5)

where $\mathbf{F}_{ij}^{e}$ is the electrostatic force from q_i to q_j; r_{ij} is the distance between the centres of the two particles and $\mathbf{n}_{ij}$ is the unit vector from q_i to q_j.

When a charged particle approaches a conducting surface, a re-distribution of the charge on the surface is induced. The charge on the particle and the induced charge on the surface cause the so-called image (charge) force [22]. The image force can be calculated as:

$$\mathbf{F}_{ps}^{I} = \frac{1}{4\pi\varepsilon_0} \frac{qq}{\left(2r_{ps}\right)^2} \mathbf{n}_{ps}$$ (6)

where $\mathbf{F}_{ps}^{I}$ is the image force between the particle and inductive surface, q is the value of the charge on the particle, r_{ps} is the distance between the centre of the particle and the inductive surface and $\mathbf{n}_{ps}$ is the unit vector.

2.3. Model setup

8

The discrete element method coupled with computational fluid dynamics (DEM-CFD) is applied to model the dynamics of particle and air in the fluidisation [23]. The particles are treated as elastic spheres. The contact interactions are modelled using the Hertz theory [24] in the normal direction and the theory of Mindlin and Deresiewicz [25] in the tangential direction. The two-way coupling scheme is used to compute interactions between particles and the fluid. The drag force is calculated according to Di Felice's correlation [23, 26]. The motion of the particle is governed by Newton's second law while the air is treated as a compressible fluid governed by continuity and momentum equations.

A 2D DEM-CFD model is set up to simulate the contact electrification and electrostatic interactions during fluidization as shown in Figure 1. In the simulation, 2500 particles with a diameter of 100 μm are used and the properties of the particles and the column are given in Table 1. The neutral particles here belong to the Group B in Geldart's group [27]. Initially the particles are randomly generated and deposited onto the base of the column with a size of $l \times h$ until the granular bed becomes stable (i.e. maximum particle velocity is smaller than 10^{-6} m·s^{-1}).

The air is then introduced through the base (inlet) of the column with a superficial gas velocities $v_g = 25 \sim 100$ mm·s^{-1}. The air is treated as a continuous compressible fluid. The internal domain is divided into 10×80 CFD cells. No-slip boundaries are assumed at the side walls, and the upper boundary (outlet) is set as a continuous outflow. The air has an average molar weight of 2.88×10^{-2} kg·mol^{-1} and a shear viscosity of 1.8×10^{-5} Pa·s. The initial air pressure is set to one atmospheric pressure and the temperature of the fluidized bed is

maintained constant at 293 K. The time setup is 3.4×10^{-8} s, which is calculated based on the highest frequency of the Rayleigh wave propagation [23].

Contact electrification and electrostatic interactions are both considered during the fluidization. Two types of particles with different work function potentials (5.9 and 4.1 V) are used. Each type has 1250 particles. The column is assumed to be conductive and have a work function potential of 3.5 V. The charging constant k_s is set to 1×10^{-4} $C \cdot m^{-2} \cdot V^{-1}$. The induced electrostatic force between particles and the image force between the particle and the wall are governed by Eqs 5 and 6, respectively. The direct truncation method [4] is applied and the cut-off distance is set to 10 particle radii. Fluidization with neutral particles, i.e. the electrification and electrostatics are ignored, are also modelled for reference and comparison.

In this 2D DEM-CFD model, the contact electrification (transferred charge) is determined in each collision, which has negligible influence on the computational time. However, the long-range electrostatic interaction can significantly prolong the computational time. The computational time with long-range electrostatic interactions is 3-5 times longer than that without the long-range interactions. A detailed comparison can be found in the literature [4]. 3D models require much more particles to produce a reasonable scale for the study due to one additional dimension. The computational time can be more significantly prolonged, especially with more particles in 3D. Therefore, the 2D model is considered in this study, and its capability to represent and analyse the electrostatic behaviours of particles in fluidization will be explored.

3. Results

3.1. The particle profiles

Figure 2 shows the fluidization process of neutral particles with a superficial gas velocity of 50 mm·s^{-1}. Initially, the granular bed is settled on the base of the column as shown in Figure 2a. When the gas is injected from the base, the particles are lifted by the gas and move upwards (Figure 2b). The granular bed is gradually fluidized. The particles are dispersed and bubbles of gas continually form and move from the base to the top. As it is assumed that the particle cannot get charged, similar bubbling behaviour as shown in Figure 2c and 2d persists throughout the entire fluidization process.

Figure 3 presents the influence of contact electrification and electrostatics on the fluidization process of chargeable particles with a superficial gas velocity of 50 mm·s^{-1}. From Figure 3a and 3b, it can be seen that at the early stage of the fluidization, the fluidized bed shows similar fluidization phenomena as that with neutral particles shown in Figure 2d. However, while the net charges on particles accumulate, bi-charged particles tend to move towards each other to form crystalline agglomerates and the gas bubbles becomes smaller (Figure 3c). As the electrostatic interaction becomes stronger and the charge accumulates, the gas cannot easily disrupt the agglomerates of bi-charged particles (Figure 3d, positive in yellow/light colour and negative in blue/dark colour). Consequently, the dispersed fluidized bed transforms into a collection of agglomerates and the gas can only flow through the channels formed between the agglomerates, rather than bubbling (Figure 3d).

3.2. The charge distribution

The charge density distribution can be used to analyze the charge accumulation and distribution during fluidization. The fluidization column is divided into 20×20 cells, and the

11

charge density of each cell is calculated as the radio of the total charge in the cell to the cell area. In this study, particles with a low work function potential are charged positively and particles with a high work function potential are charged negatively as observed in Figure 3. The positive and negative charge can be analysed separately to examine the charge distribution. The positive charge density distribution only considers the total positive charge of the fluidized bed and the negative charge density distribution is only for the negative charge.

Figures 4 and 5 show the corresponding positive and negative charge density distributions in the fluidized bed with a superficial gas velocity of 50 mm·s^{-1}. Both positive and negative charge density distributions present similar patterns and accumulation processes during the fluidization. At the early stage of the fluidization, the particles start to acquire charges. However, the charge density is relatively low (Figures 4a and 5a), and thus the granular bed can still be fluidized (Figure 3b). As the granular bed is fluidized, the charge density increases (Figures 4b and 5b). In addition, the positive and negative charges are concentrated in the same areas in the fluidized bed (Figures 4c and 5c), which indicates that the positive and negative charges induce strong electrostatic interactions to form agglomerates of particles (Figure 3d).

Figure 6 shows the fluidized beds of charged particles with various superficial gas velocities at $t = 3.4$ s, at which a steady fluidization state is reached. It is clear that the structures and the height of fluidized beds for chargeable particles vary with the superficial gas velocities. With gas velocities of $v_g = 25$ and 50 mm·s^{-1}, the granular beds form large agglomerates and the gas cannot disrupt the agglomerates but only flows through the channels between agglomerates. On the contrary, a gas velocity of 100 mm·s^{-1} can lead to impacts between

agglomerates and also breakage. Therefore, due to the breakage and fluidization, the heights of fluidized beds increase with the superficial gas velocity.

Figure 7 shows the corresponding positive charge density distribution of charged particles with various gas velocities at 3.4 s. The fluidized beds with different gas velocities present different charge density patterns. At a smaller gas velocity (say, 25 mm·s^{-1}), the charge density is smaller and concentrated at the top-centre of the granular bed. When the superficial gas velocity is 50 mm·s^{-1}, the charge is distributed over the entire granular bed densely, which means that the agglomerates are relatively stable as shown in Figure 7b. As the gas velocity is much larger, the charge is distributed sparsely in the fluidized bed since the particles and agglomerates are moving with the gas flow (Figure 7c). These phenomena indicate that the superficial gas velocity can affect the contact electrification process, and the subsequent dynamics of particles and agglomeration caused by electrostatic interactions. The negative charge density distribution is very similar to the positive charge density distribution.

The net charge is defined as the summation of the positive and negative charges, which represents the polarity and the total charge of the fluidized bed. The net charge density can be calculated as the net charge of particles in each grid divided by the area of the grid. Figure 8 presents the corresponding net charge density distribution of charged fluidized beds with various gas velocities at t=3.4 s. It can be seen that the net charges of fluidized beds with various gas velocities are negative, as the work functions of the particles are all higher than that of the column (see Discussion). A higher gas velocity causes a more dispersed and sparse net charge distribution. Compared to Figure 7, the value of net charge density is much smaller than the corresponding positive charge density of the fluidized bed.

3.3. The charge accumulation

Figure 9 presents the charge accumulation of particles caused by contact electrification during fluidization. It is as expected that the charge of neutral particles stays zero during fluidization. The fluidization with chargeable particles show different charging processes due to contact electrification. As shown in Figure 9a, initially, the positive charge of the fluidized bed with smaller gas velocity of 25 mm·s^{-1} increases faster than that with larger gas velocity (50 and 100 mm·s^{-1}). However, after a period of fluidization, the accumulation of positive charge at higher gas velocities becomes faster and exceeds that at a smaller gas velocity. The total negative charges in Figure 9b shows similar trends. The total net charges in all cases with contact electrification are negative (Figure 9c), as the work functions of the particles are all higher than that of the column. In addition, the total net charge increases faster at a higher superficial gas velocity.

3.4. The performance of fluidization

Figure 10 shows the mean coordination number of the fluidized bed during fluidization. For the fluidized bed without contact electrification, the coordination number is nearly zero, which indicates that the granular bed is fully dispersed and fluidized at the superficial gas velocity of 50 mm·s^{-1}. However, for the fluidized bed with chargeable particles, the coordination number gradually increases during fluidization. Moreover, when a smaller gas velocity is used, a faster increase and a larger coordination number are induced, implying that the particles retain a larger number of contacts during fluidization at a smaller superficial gas velocity.

14

Figure 11 shows the corresponding collision rate of neutral and chargeable particles during fluidization. The collision rate is defined as the derivative of the total number of collision over time, which also represents the breakage of contacts (or agglomerates) during fluidization. The collision rates of neutral and chargeable particle systems demonstrate different features. For neutral particles, once the fluidization is achieved, the collision rate is low but stable. However, for the chargeable particle system, the collision (breakage) rate initially increases due to the formation and breakage of agglomerates caused by electrostatic forces. At smaller gas velocities (25 and 50 mm·s^{-1}), the collision rate of the chargeable particle system starts to decreases when the electrostatic attractive force is strong enough to hold agglomerates together. At a higher gas velocity (100 mm·s^{-1}), the gas is still able to induce breakage of agglomerates. Therefore, a large fluctuation of collision (breakage) rate is observed for the chargeable particle system at a higher gas velocity.

The granular temperature is usually used to reflect the fluctuating energy inside a particle system, which can be defined as:

$$T_g = \frac{1}{D_n} \left\langle (\mathbf{v} - \overline{\mathbf{v}})^2 \right\rangle \tag{7}$$

where D_n is the spatial dimension, which is 2 for 2D in this study; $\mathbf{v}$ is the velocity of each particle; $\overline{\mathbf{v}}$ is the average velocity of particles; the angle bracket $\left\langle\right\rangle$ indicates ensemble average. Generally, a higher granular temperature represents a high degree of mixing in the particle system.

Figure 12 presents the granular temperature of neutral and chargeable particles during fluidization. For neutral particles, the granular temperature gradually increases to a relatively

15

stable level. A higher superficial gas velocity (50 mm·s^{-1}) leads to a higher granular temperature than a smaller velocity (25 mm·s^{-1}). For chargeable particles, the granular temperature initially increases. However, as fluidization continues, at smaller gas velocities (25 and 50 mm·s^{-1}), the granular temperature decreases due to agglomeration between charged particles. At higher gas velocity (100 mm·s^{-1}), the granular temperature can be maintained as the fluidization can break agglomerates of charged particles. In addition, with the same gas velocity, the granular temperature of chargeable particles is relatively lower than that of neutral particles, indicating that the fluctuating energy in the chargeable particle system is lower than that in the neutral particle system.

The pressure drop of the fluidization, which can be used to identify the performance of the fluidization, is defined as the pressure different between the pressure of the input gas at the base of the fluidized bed and the pressure of the outflow gas at the top of the fluidized bed. Figure 13 shows the pressure drops of the fluidized bed with the neutral and chargeable particles at a superficial gas velocity of 50 mm·s^{-1}. It can be seen that, for both cases, the pressure drop increases rapidly to a plateau once the gas is injected. The pressure drop of the fluidized bed with neutral particles continues to fluctuate as the neutral particles are moving upwards and downwards in the fluidization. However, the pressure drop of the fluidized bed with chargeable particles becomes relatively steady, indicating that the movement of the particles with the gas is relatively small.

Figure 14 shows the pressure drops of fluidized beds with neutral particles at various gas velocities. The evolution of the pressure drops for all cases show similar trends during fluidization. The pressure drop initially increases rapidly and then reaches a plateau. The pressure drop keeps fluctuating due to the movement of the neutral particles.

Figure 15 shows the pressure drops of fluidized beds with chargeable particles at various gas velocities. For all case, the pressure drops show a similar trend to that shown in Figure 13. For the cases with smaller gas velocities (25 and 50 mm·s^{-1}), the pressure drop rapidly increases to a plateau. However, at a higher gas velocity of 100 mm·s^{-1}, a fluctuating pressure drop during the fluidization is observed, indicating that particles are moving with the gas at high gas velocities.

4. Discussion

4.1. The charging process during fluidization

Since two types of particles with different work function potentials are used, both positive and negative charges are observed in the fluidized bed with chargeable particles. During a contact, the particles with a higher work function will be charged negatively and those with a lower work function are positive. At the initial stage of fluidization, a fluidized bed with a lower gas velocity is less dispersed and has more contacts between particles than that with a higher gas velocity, which leads to a faster increase in the total positive (negative) charge. However, as the charge accumulates on the particles, the electrostatic interactions become stronger and force particles to form agglomerates. The interactions become so strong that the gas with a small velocity (25 mm·s^{-1}) cannot disrupt the agglomerates (Figures 6a and 10). Due to the agglomeration, fewer collisions occur between particles and the charge transfer is also limited for particles within the agglomerate. Thereafter, the positive (negative) charge accumulation becomes slower for the case with a lower gas velocity (25 mm·s^{-1}) than those with higher gas velocities, which can still break the agglomerates and keep fluidizing the

17

granular bed. The charging process during fluidization with bi-charged particles varies with the particle properties (e.g. work functions) and the operating conditions (e.g. the gas velocity) due to the combined effects of the contact electrification and electrostatic interactions. However, for fluidization with mono-charged particles without considering the electrostatic interactions [11], the charging process shows an exponential pattern. Therefore, the sensitivity of the charging process to the combined effects of the contact electrification and electrostatics requires further investigated.

4.2. Agglomeration during fluidization

The bi-charged particles can form agglomerates due to electrostatic interactions during fluidization. The size and the breakage of the agglomerates are determined by the superficial gas velocity. A higher gas velocity can lead to a higher impact velocity between agglomerates and result in the disruption of the agglomerates as shown in Figure 6. Hence, the corresponding coordination number is smaller at a higher gas velocity as shown in Figure 10, indicating that a smaller number of particles adhere to each other. Moreover, the size of the agglomerate at a higher gas velocity is smaller. The adhesion of particles on the walls is also observed, especially at a higher gas velocity (see Figure 6c), in which a few layers of particles are attached to the wall instead of moving with the gas flow. It can be seen, although the neutral particles at the Group B in Geldart's group [27] can be fluidized, the bi-charged particles behave like cohesive particles in Group C in Geldart's group due to the electrostatic interactions. Bi-charged particles and induced agglomerate are commonly observed in experiments [1, 7, 8, 28]. Mono-sized particles with positive and negative charges tend to form agglomerates with regular lattice, i.e. crystalline structure, depending on the number of

particles, electrostatic interactions and dynamics of the process. The current study shows a broad agreement with these phenomena as can be seen in Figures 3 and 6.

4.3. The performance of fluidization

Contact electrification and subsequent electrostatic interaction can affect the overall performance of the fluidization. As can be seen from Figure 2, a superficial gas velocity of 50 mm·s^{-1} can fully fluidize the granular bed considered in this study. However, the chargeable particles cannot be fully fluidized as shown in Figures 3, 6b and 11. The phenomena are also reflected by the fluctuation of the pressure drop (see Figures 13-15). When particles are fluidized and moving with the gas bubbles, the pressure drop tends to fluctuate, which is induced by accelerating and moving the particles. However, for charged particles with a smaller gas velocity, the agglomerates are too large to be lifted by the gas. As a result, the gas can only flow through the channels formed by the agglomerates, which leads to a steady gas flow and a steady pressure drop rather than a fluctuation. The high gas velocity (100 mm·s^{-1}) can disrupt the agglomerates and keep fluidizing the granular bed, which needs extra energy and cause a large pressure drop as shown in Figure 15. The agglomeration clearly affects the pressure drop and increases the minimum bubbling velocity, which shows a qualitative agreement with the experimental results reported in the literature [8,14].

4.4. The charge distribution

The charge distribution can also be affected by the different fluidization behaviours at different gas velocities. A small gas velocity (25 mm·s^{-1}) cannot fully fluidize the chargeable particles when the combined effects of contact electrification and electrostatics is activated.

Due to the formation of agglomerates, the movement of particles at the base are restricted by the electrostatic forces and the gravity of the granular bed. Therefore, the charge density in this region is much lower as shown in Figure 7a. A higher gas velocity (50 mm·s^{-1}) can maintain the fluidization longer as indicated by the coordination number and collision rate in Figures 10 and 11, which results in a more uniform charge transfer process in the fluidized bed (Figure 7b). When the gas velocity is increased to 100 mm·s^{-1}, the gas can break the agglomerates of charged particles and mobilize the particles and the agglomerates. Thus, the charge distribution is much sparse in the fluidized bed. The charge distribution in the bi-charged particle system is different from the mono-charged system, especially when the electrostatic force is negligible. In the mono-charged particle system, the charge is initially generated and transferred between particles and column walls, and then propagates from the region close to walls to the centre during fluidization [11]. LaMarche et al. [13] observed similar phenomena in experiments, in which the charge on particles close to the wall is higher than that in the centre when particles flow through a cylinder and become charged. However, when a mixture of bi-charged particles is involved, the charge distribution becomes more complex. In this study, the positive and negative charges of mono-sized particles distribute sparsely uniform. When the size and electric properties of particles are different, more complex distributions of charge and particles are observed in experiments, including coating and segregation [13].

4.5. The effect of the column

The material properties, especially work function, of the column can also affect the charging process during fluidization. According to Eqs (3.1) and (3.7), the total potential difference between the particle and the column surface will eventually become zero if there are

sufficient contacts between the particle and the column. Since the work function potentials of the particles are higher than the work function potential of the column, the total charge of the granular bed becomes negative. In addition, with a larger superficial gas velocity, particles have a greater probability of making contact with the column and therefore have a larger total net charge. However, the agglomerates restrict the movement of the particles and reduce the contact number between the particle and the column. The increase of the total charge is very slow and the absolute value of the total charge is much smaller than the total positive charge as shown Figure 9, especially for the cases with lower gas velocities. Moreover, it can be seen that a layer of agglomerates is generated and attracted along each side of the column because of the contact electrification and the image force between the particle and the column, which will decrease and prevent further charge transfer from the column to the particle. Therefore, it will take a much longer time (or even not possible) to achieve the theoretical equilibrium state of the total charge as indicated by Eqs. (1) and (2). Clearly, the column wall plays a significant role in the charging process, which has been observed in the experiments [13, 29]. The interplay between walls and particles, including material properties and size effects need further investigations.

5. Conclusions

A DEM model with contact electrification and electrostatic interactions is developed to analyse the effect of electrostatics on fluidization. Particles with two different work functions and fluidization at different superficial gas velocities are considered. It is found that the fluidization process is influenced by contact electrification and electrostatic interactions. In addition, the gas velocity plays a significant role in the charging and agglomeration processes during fluidisation.

Particles with different work functions are charged positively and negatively. The charged particles form agglomerates, which can inhibit the fluidization process. A charged granular bed at a lower gas velocity cannot be fluidized because of the presence of agglomerates. A higher gas velocity can break the agglomerates and drag the primary particles to move in the fluidized bed, which leads to a larger charge accumulation and a sparse charge distribution. The difference in work functions between the column and the particles can also affect the particle charging behaviour during fluidization. Further analysis and discussion of these phenomena are required.

References

[1]   S. Matsusaka, H. Maruyama, T. Matsuyama, M. Ghadiri, Triboelectric charging of powders: A review, Chem. Eng. Sci. 65 (2010) 5781–5807.

[2]   E.N. Nwose, C. Pei, C.-Y. Wu, Modelling die filling with charged particles using DEM/CFD, Particuology. 10 (2012) 229–235.

[3]   C. Pei, C.-Y. Wu, S. Byard, D. England, Numerical analysis of electrostatic effects during powder deposition using DEM/CFD, J. Pharm. Pharmacol. 62 (2010) 1454–1455.

[4]   C. Pei, C.-Y. Wu, D. England, S. Byard, H. Berchtold, M. Adams, DEM-CFD modeling of particle systems with long-range electrostatic interactions, AIChE J. 61 (2015) 1792–1803. doi:10.1002/aic.14768.

[5]   Y. Pu, M. Mazumder, C. Cooney, Effects of electrostatic charging on pharmaceutical powder blending homogeneity, J. Pharm. Sci. 98 (2009) 2412–2421.

[6]   J. Guardiola, V. Rojo, G. Ramos, Influence of particle size, fluidization velocity and relative humidity on fluidized bed electrostatics, J. Electrostat. 37 (1996) 1–20.

[7]   A. Wolny, W. Kaźmierczak, Triboelectrification in fluidized bed of polystyrene, Chem. Eng. Sci. 44 (1989) 2607–2610. doi:10.1016/0009-2509(89)85204-2.

[8]   A. Wolny, W. Kaźmierczak, The influence of static electrification on dynamics and rheology of fluidized bed, Chem. Eng. Sci. 48 (1993) 3529–3534. doi:10.1016/0009-2509(93)85008-D.

[9]   Q. Zhang, Y. Zhou, J. Wang, B. Jiang, Y. Yang, S. Stapf, et al., Particle Motion in Two- and Three-Phase Fluidized-Bed Reactors Determined by Pulsed Field Gradient Nuclear Magnetic Resonance, Chem. Eng. Technol. 38 (2015) 1269–1276. doi:10.1002/ceat.201400659.

[10]   Z. Liu, X.T. Bi, J.R. Grace, Electrostatic charging behaviour of dielectric particles in a pressurized gas–solid fluidized bed, J. Electrostat. 68 (2010) 321–327.

[11]   C. Pei, C.-Y. Wu, D. England, S. Byard, H. Berchtold, M. Adams, Numerical analysis of contact electrification using DEM–CFD, Powder Technol. 248 (2013) 34–43. doi:10.1016/j.powtec.2013.04.014.

[12]   M.A. Hassani, R. Zarghami, H.R. Norouzi, N. Mostoufi, Numerical investigation of effect of electrostatic forces on the hydrodynamics of gas–solid fluidized beds, Powder Technol. 246 (2013) 16–25. doi:10.1016/j.powtec.2013.05.007.

[13]   K.R. LaMarche, X. Liu, S.K. Shah, T. Shinbrot, B.J. Glasser, Electrostatic charging during the flow of grains from a cylinder, Powder Technol. 195 (2009) 158–165.

[14]   K. Dong, Q. Zhang, Z. Huang, Z. Liao, J. Wang, Y. Yang, Experimental investigation of electrostatic effect on bubble behaviors in gas-solid fluidized bed, AIChE J. 61 (2015) 1160–1171.

[15]   E.W.C. Lim, Mixing Behaviors of Granular Materials in Gas Fluidized Beds with

Electrostatic Effects, Ind. Eng. Chem. Res. 52 (2013) 15863–15873. doi:10.1021/ie402511p.

[16]   T. Matsuyama, H. Yamamoto, Characterizing the electrostatic charging of polymer particles by impact charging experiments, Adv. Powder Technol. 6 (1995) 211–220.

[17]   J. Lowell, A.C. Roseinnes, Contact electrification, Adv. Phys. 29 (1980) 947–1023.

[18]   C. Pei, C.-Y. Wu, M. Adams, Numerical analysis of contact electrification of non-spherical particles in a rotating drum, Powder Technol. 285 (2015) 110–122. doi:10.1016/j.powtec.2015.05.050.

[19]   S. Matsusaka, M. Ghadiri, H. Masuda, Electrification of an elastic sphere by repeated impacts on a metal plate, J. Phys. D. Appl. Phys. 33 (2000) 2311–2319.

[20]   H. Watanabe, M. Ghadiri, T. Matsuyama, Y.L. Ding, K.G. Pitt, H. Maruyama, et al., Triboelectrification of pharmaceutical powders by particle impact, Int. J. Pharm. 334 (2007) 149–155.

[21]   C. Pei, C.Y. Wu, M. Adams, D. England, S. Byard, H. Berchtold, Contact electrification and charge distribution on elongated particles in a vibrating container, Chem. Eng. Sci. 125 (2015) 238–247. doi:10.1016/j.ces.2014.03.014.

[22]   J.P.K. Seville, U. Tüzün, R. Clift, Processing of particulate solids, Blackie Academic & Professional, London, 1997.

[23]   K.D. Kafui, C. Thornton, M.J. Adams, Discrete particle-continuum fluid modelling of gas-solid fluidised beds, Chem. Eng. Sci. 57 (2002) 2395–2410.

[24]   K.L. Johnson, Contact Mechanics, Cambridge University Press, Cambridge, 1985.

[25]   R.D. Mindlin, H. Deresiewicz, Elastic spheres in contact under varying oblique forces, J. Appl. Mech. ASME. 20 (1953) 327–344.

[26]   R. Di Felice, The voidage function for fluid-particle interaction systems, Int. J. Multiph. Flow. 20 (1994) 153–159.

[27]   D. Geldart, Types of gas fluidization, Powder Technol. 7 (1973) 285–292.

[28]   B.A. Grzybowski, A. Winkleman, J.A. Wiles, Y. Brumer, G.M. Whitesides, Electrostatic self-assembly of macroscopic crystals using contact electrification., Nat. Mater. 2 (2003) 241–245. doi:10.1038/nmat860.

[29]   H. Watanabe, M. Ghadiri, T. Matsuyama, Y.L. Ding, K.G. Pitt, H. Maruyama, et al., Triboelectrification of pharmaceutical powders by particle impact, Int. J. Pharm. 334 (2007) 149–155.
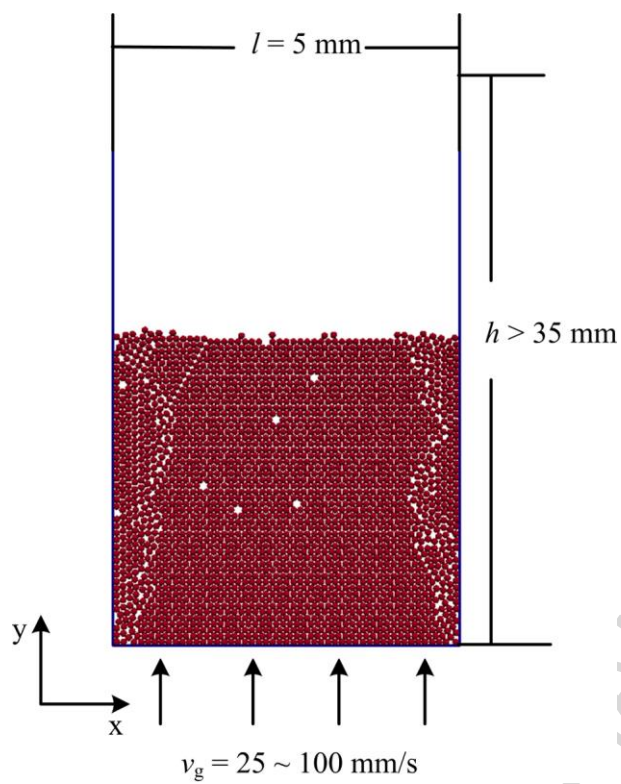
Figure 1
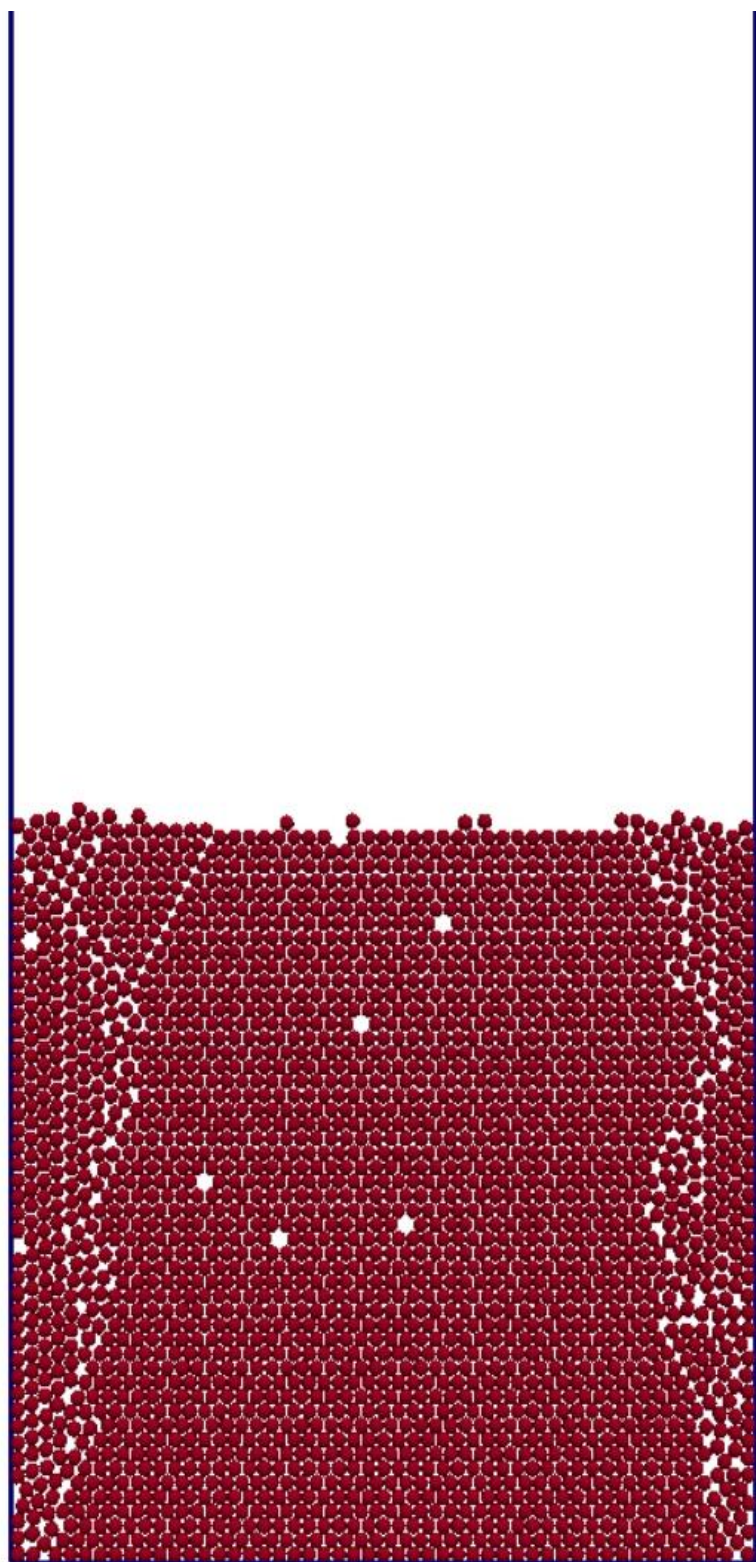
(a) $t = 0.0$ s

Figure 2a
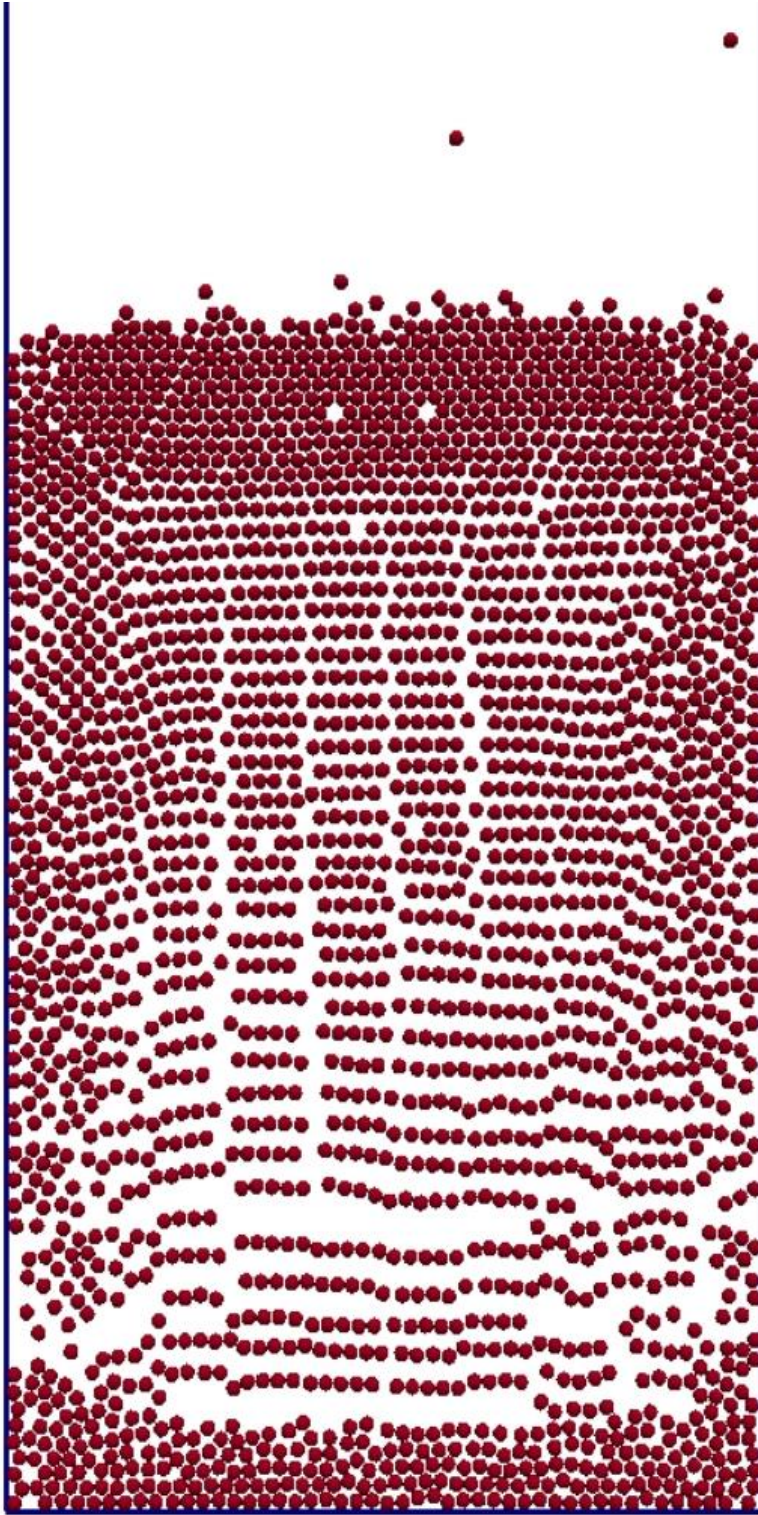
(b) $t = 0.068$ s

Figure 2b
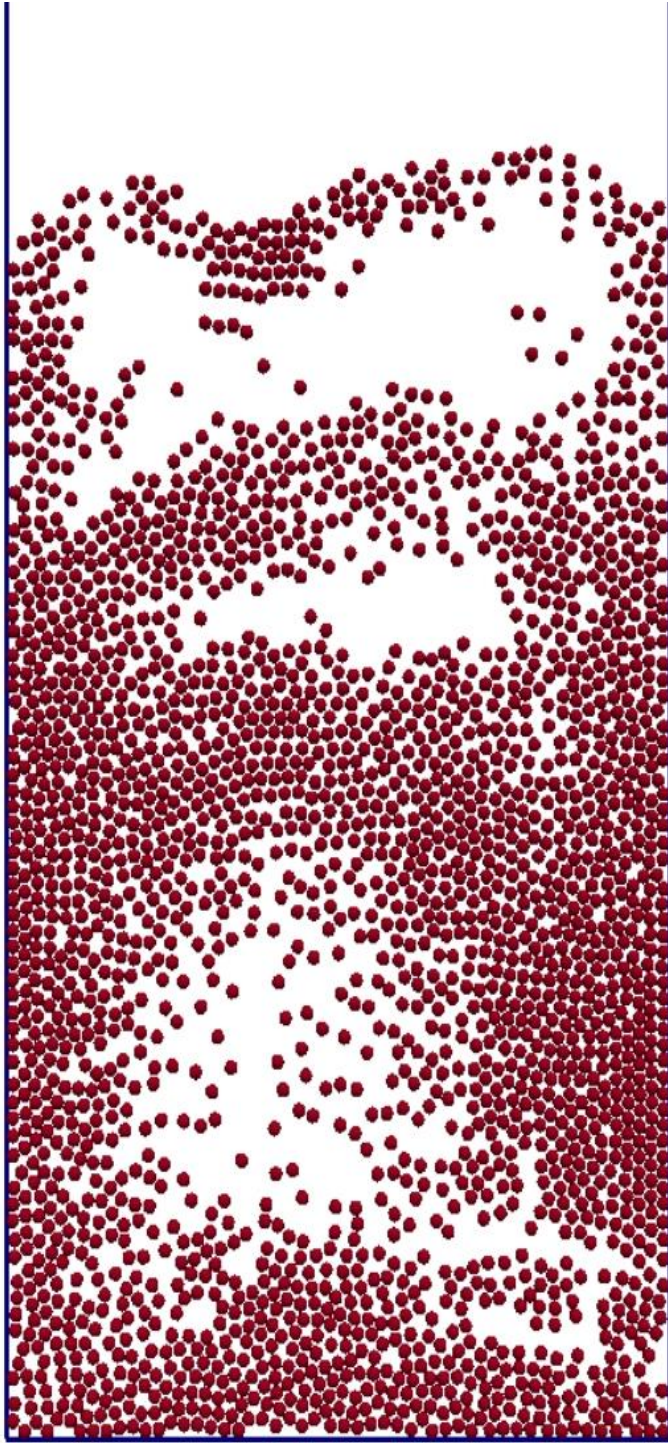
(c) $t = 0.17$ s

Figure 2c
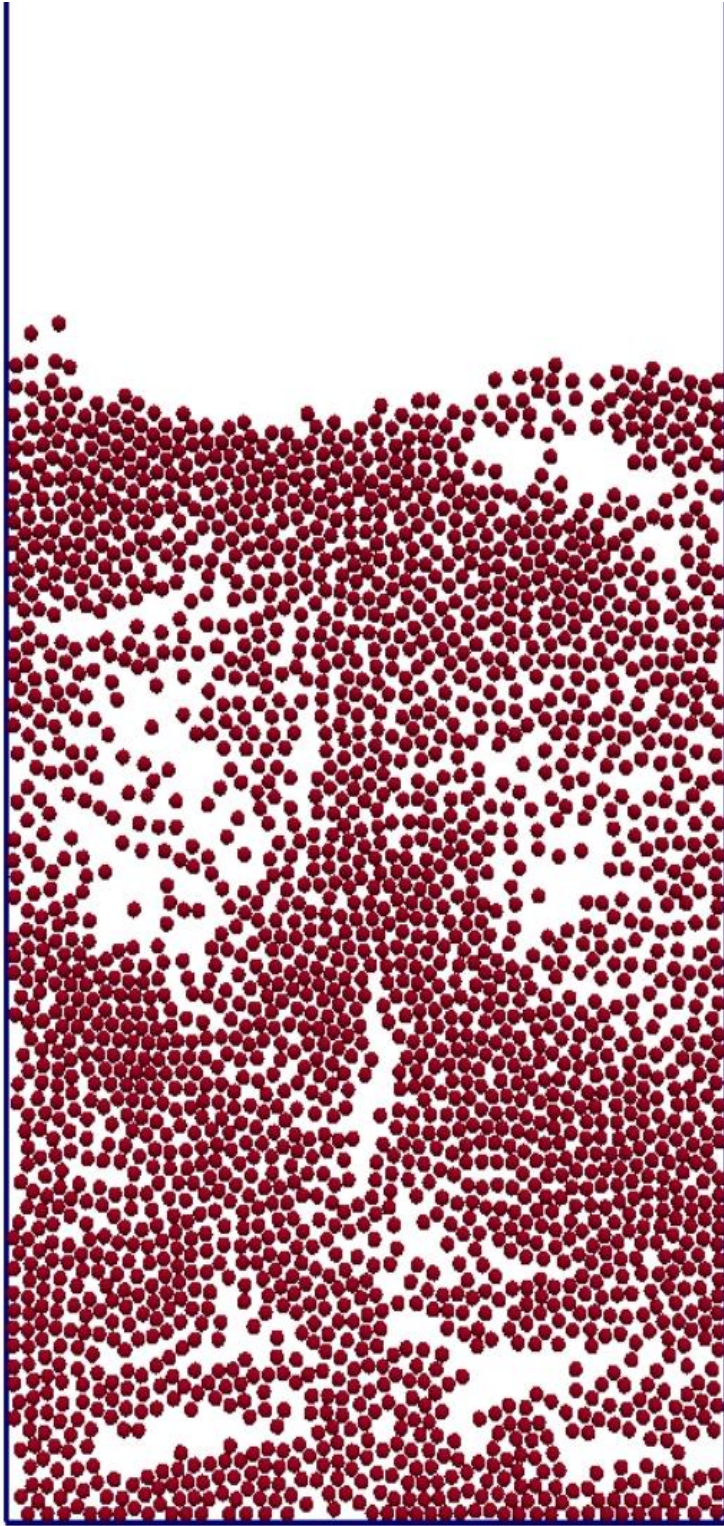
(d) $t = 0.34$ s

Figure 2d
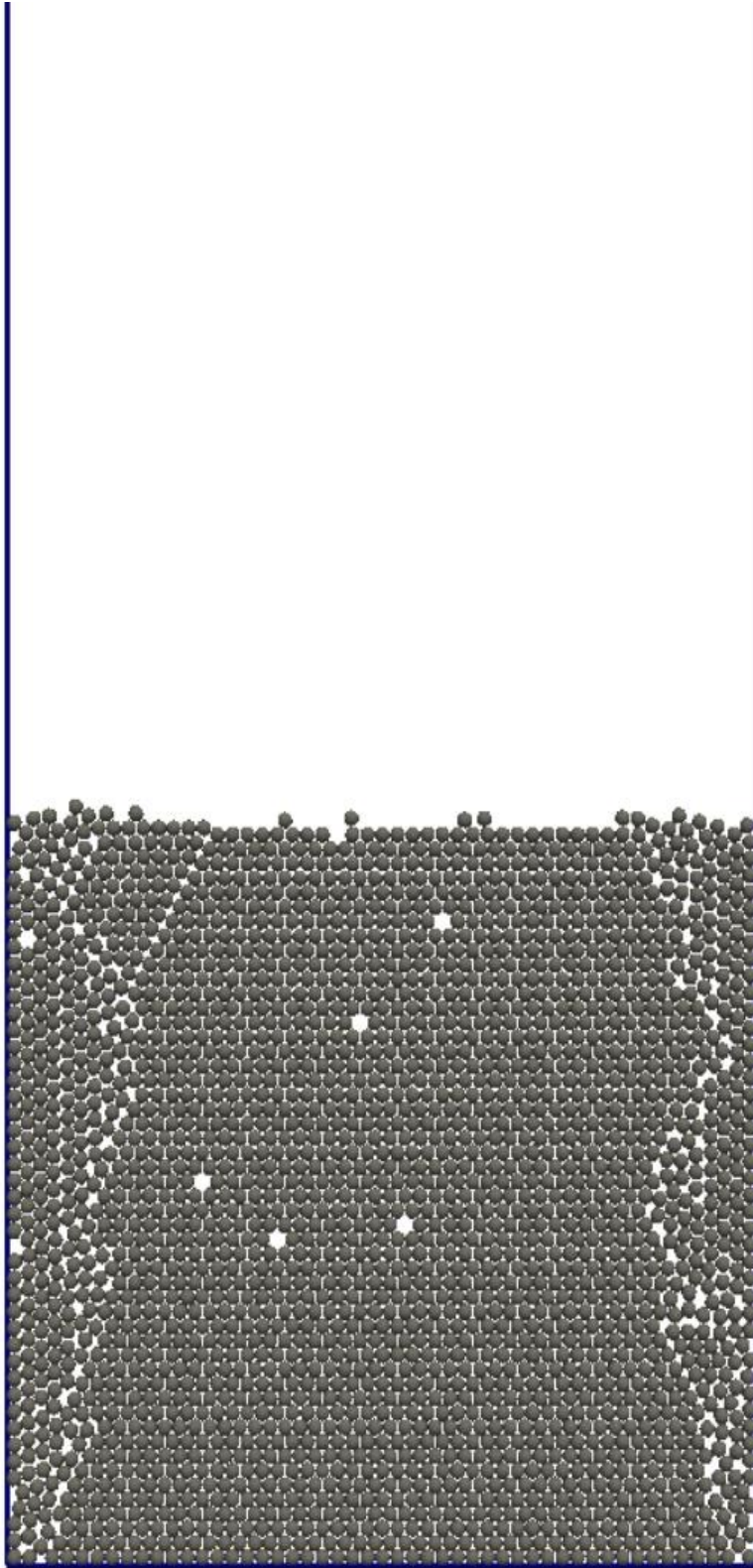
(a) $t = 0.0$ s

Figure 3a
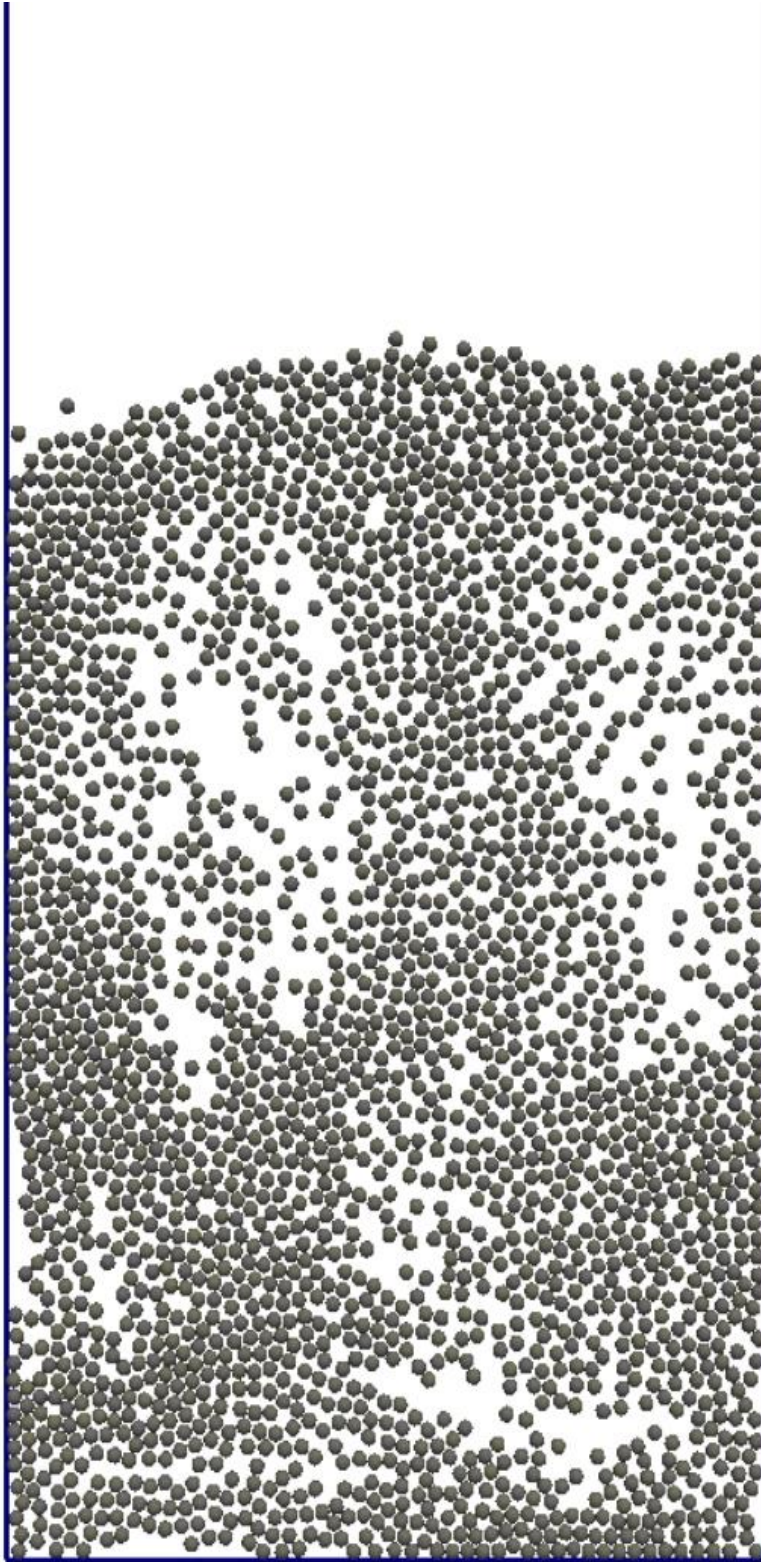
(b) $t = 0.34$ s

Figure 3b
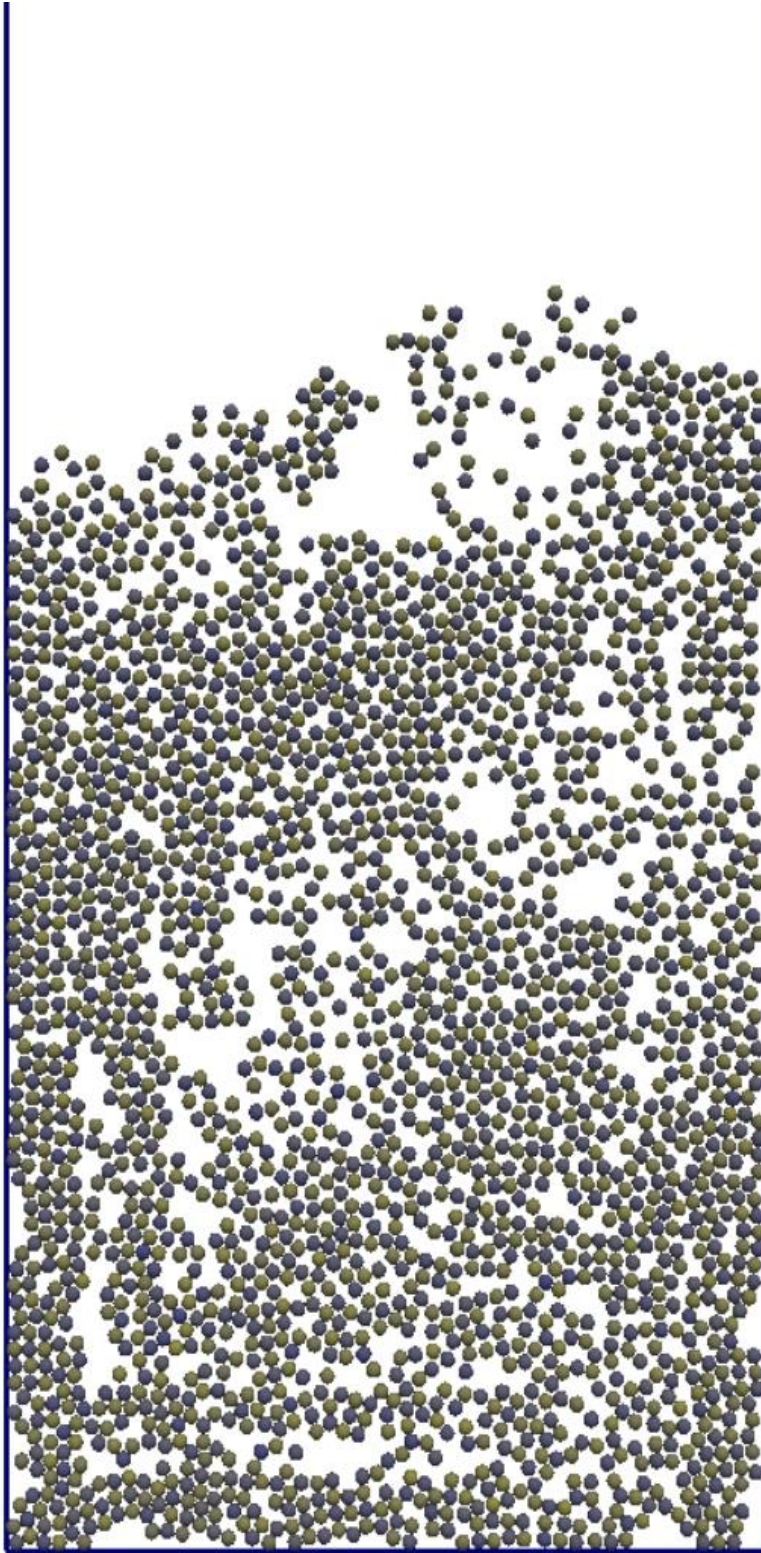
(c) $t = 1.02$ s

Figure 3c
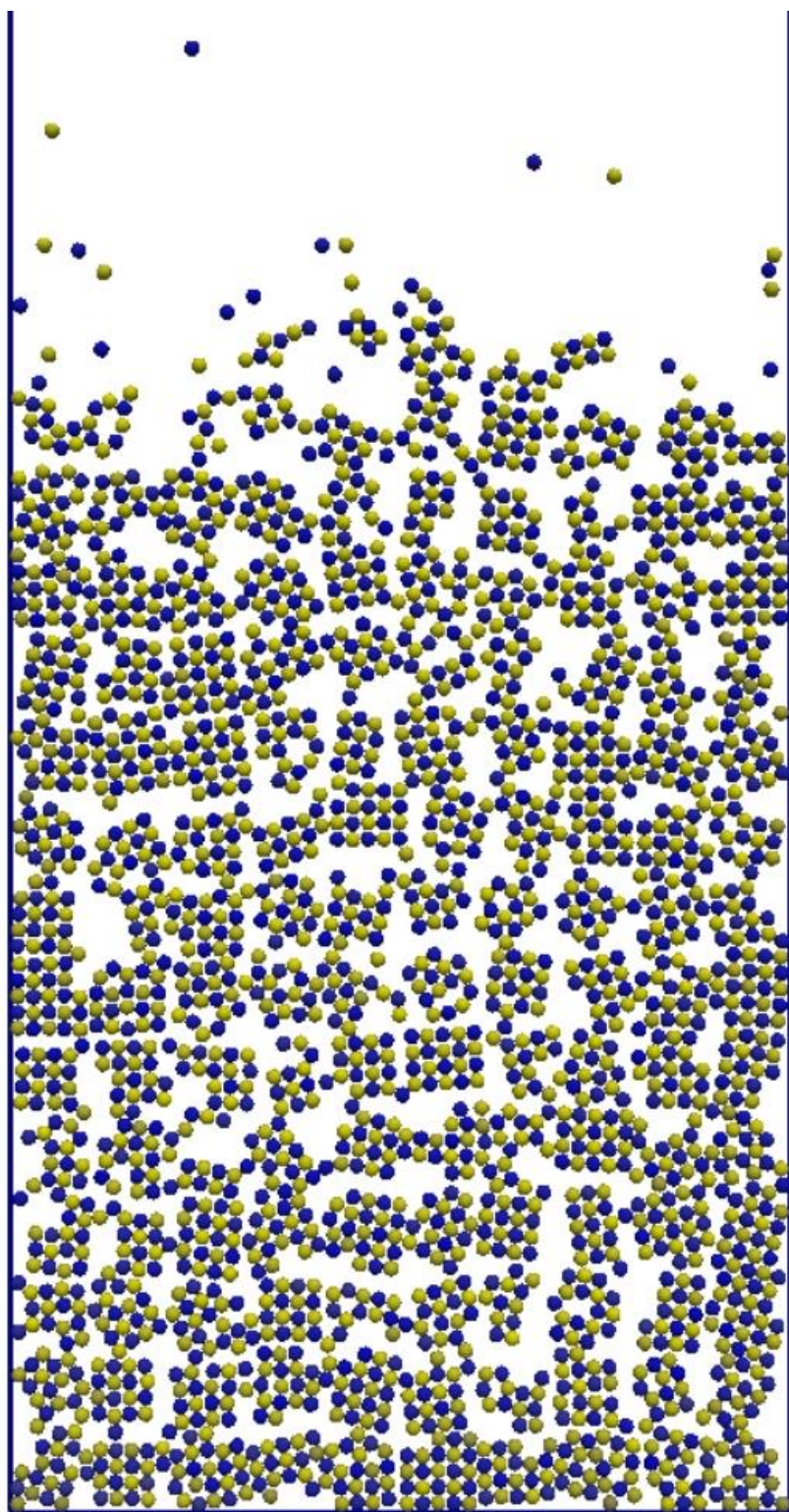
(d) $t = 2.05$ s

Figure 3d
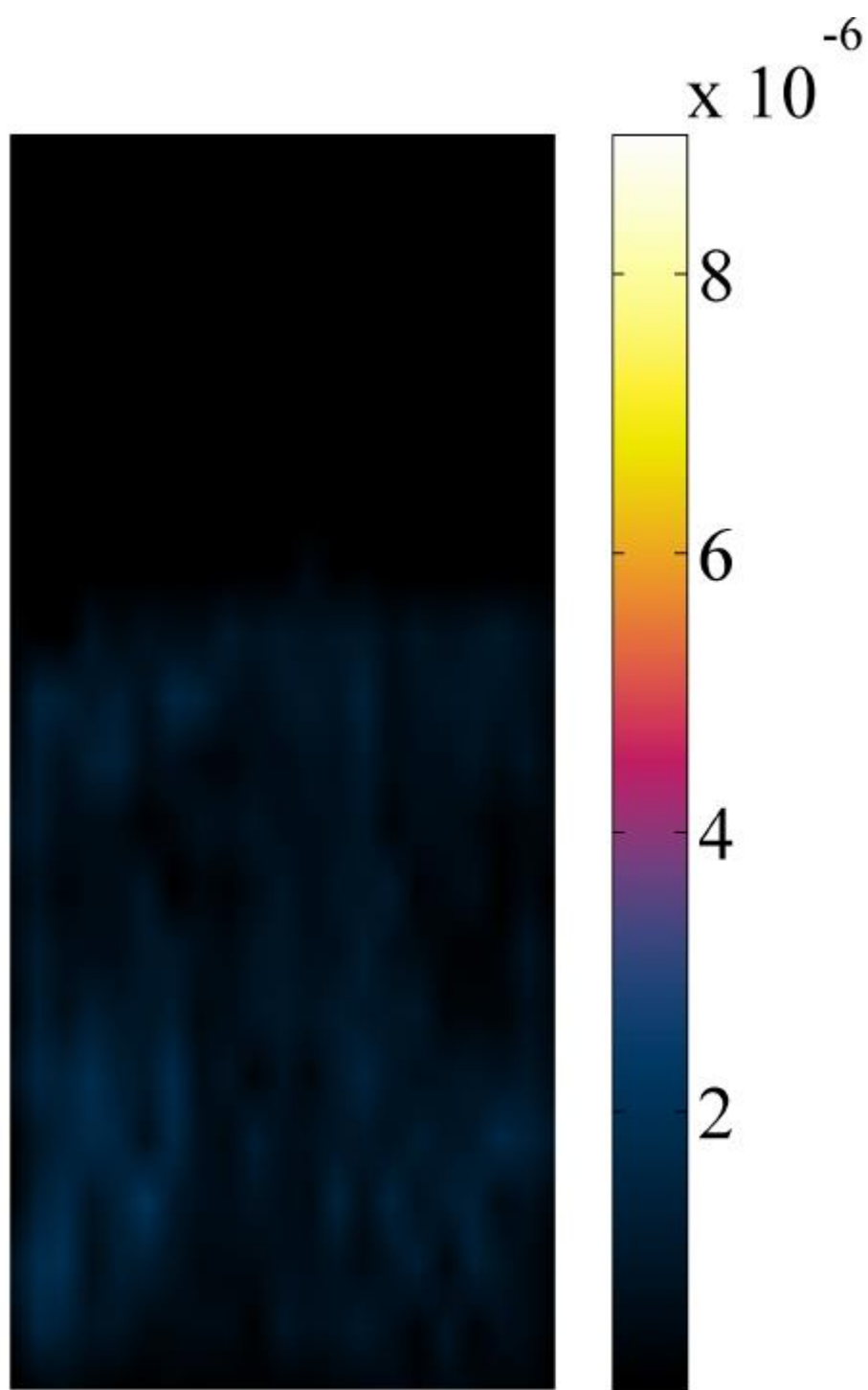
(a) $t = 0.34$ s

Figure 4a

(b) $t = 1.02$ s

Figure 4b

(c) $t = 2.05$ s

Figure 4c

(a) $t = 0.34$ s
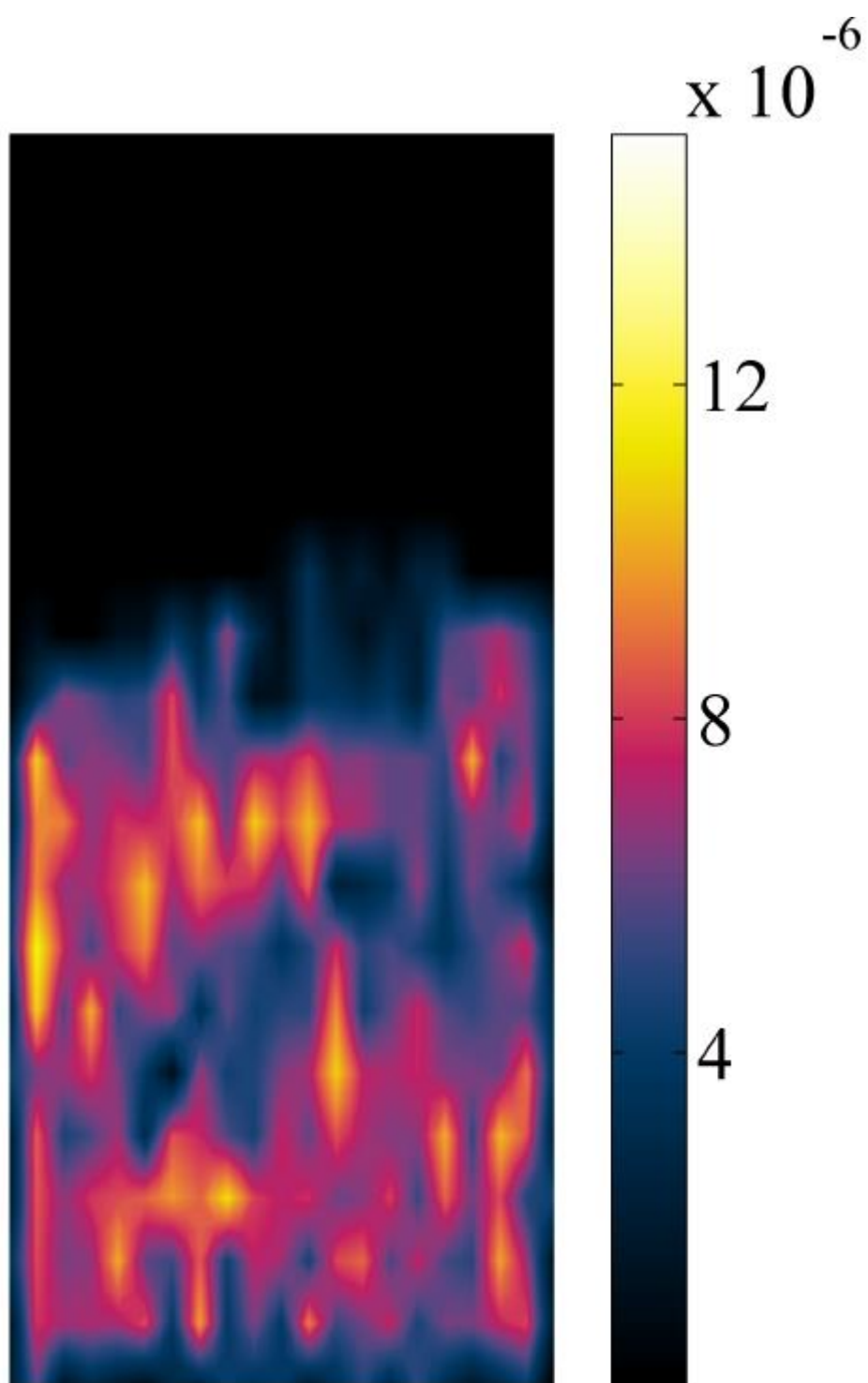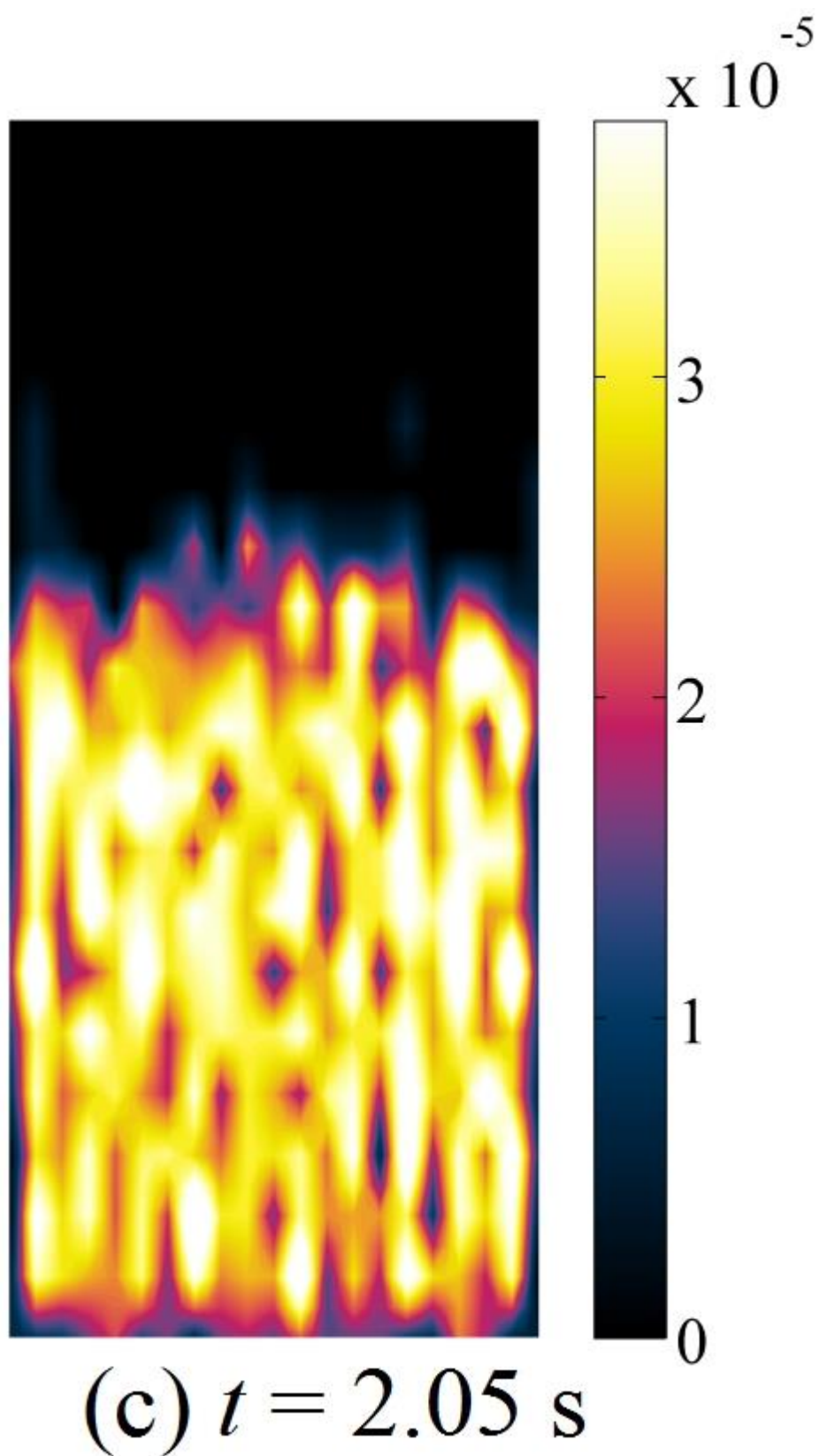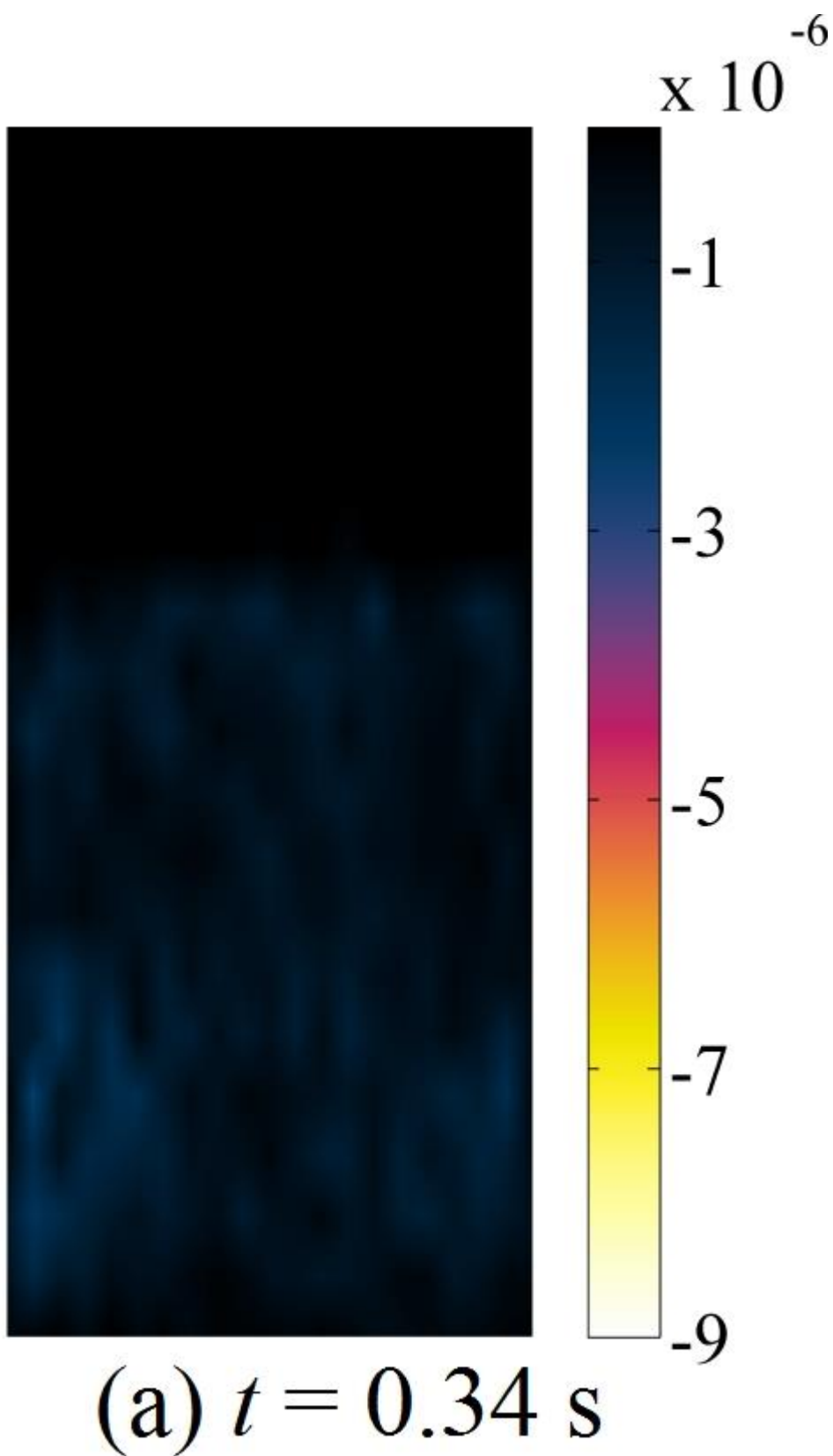
Figure 5a

(b) $t = 1.02$ s

Figure 5b

(c) $t = 2.05$ s
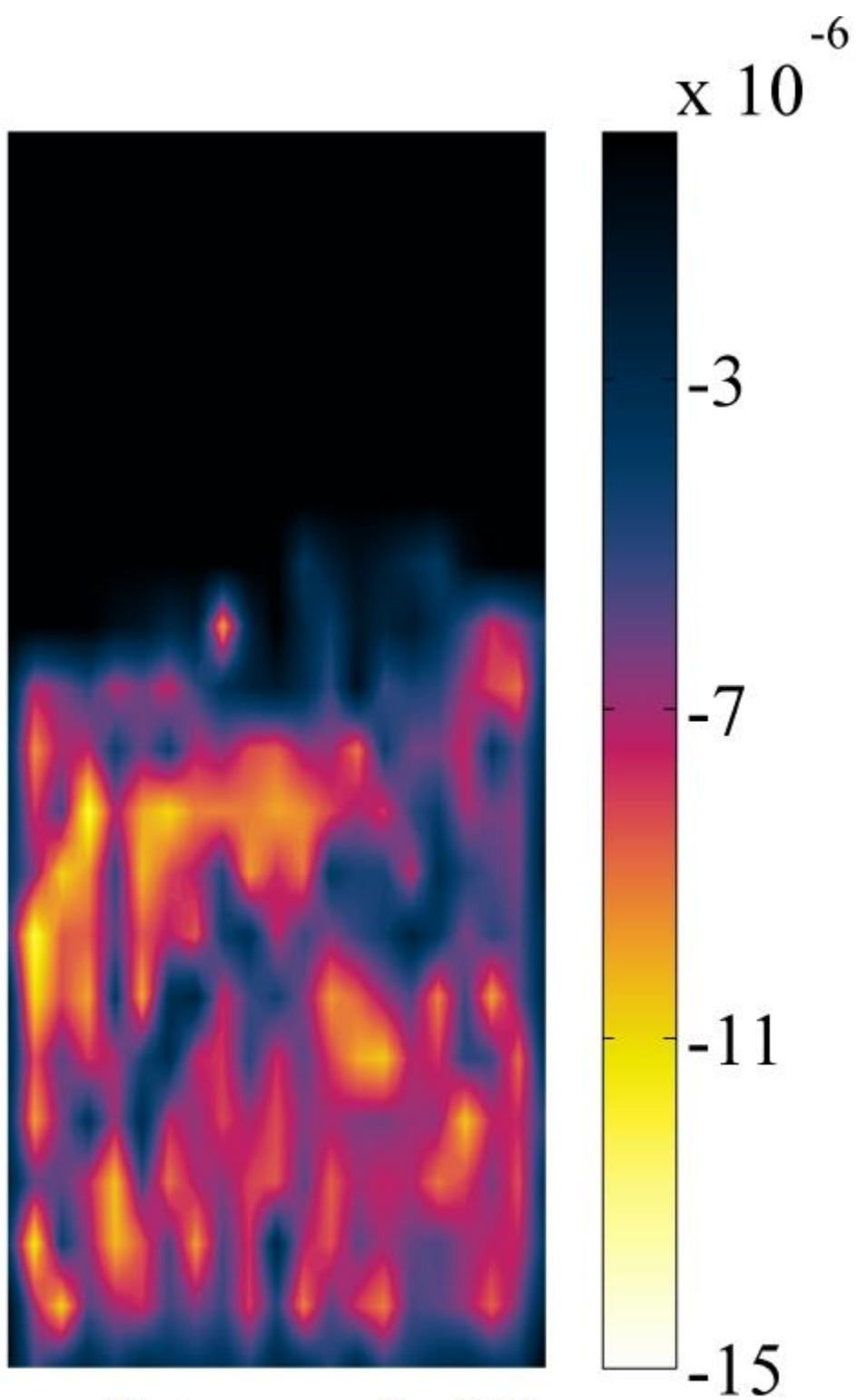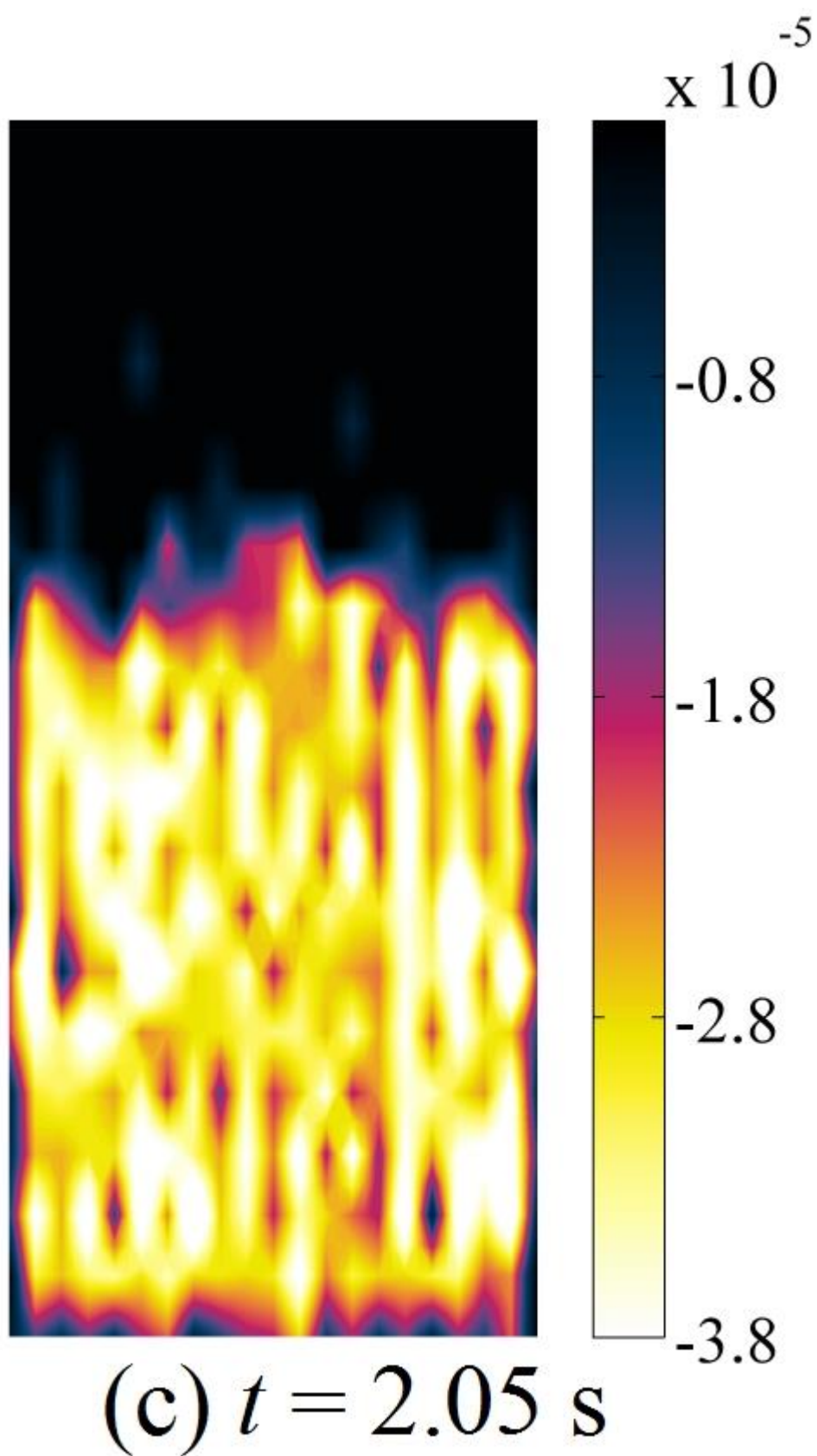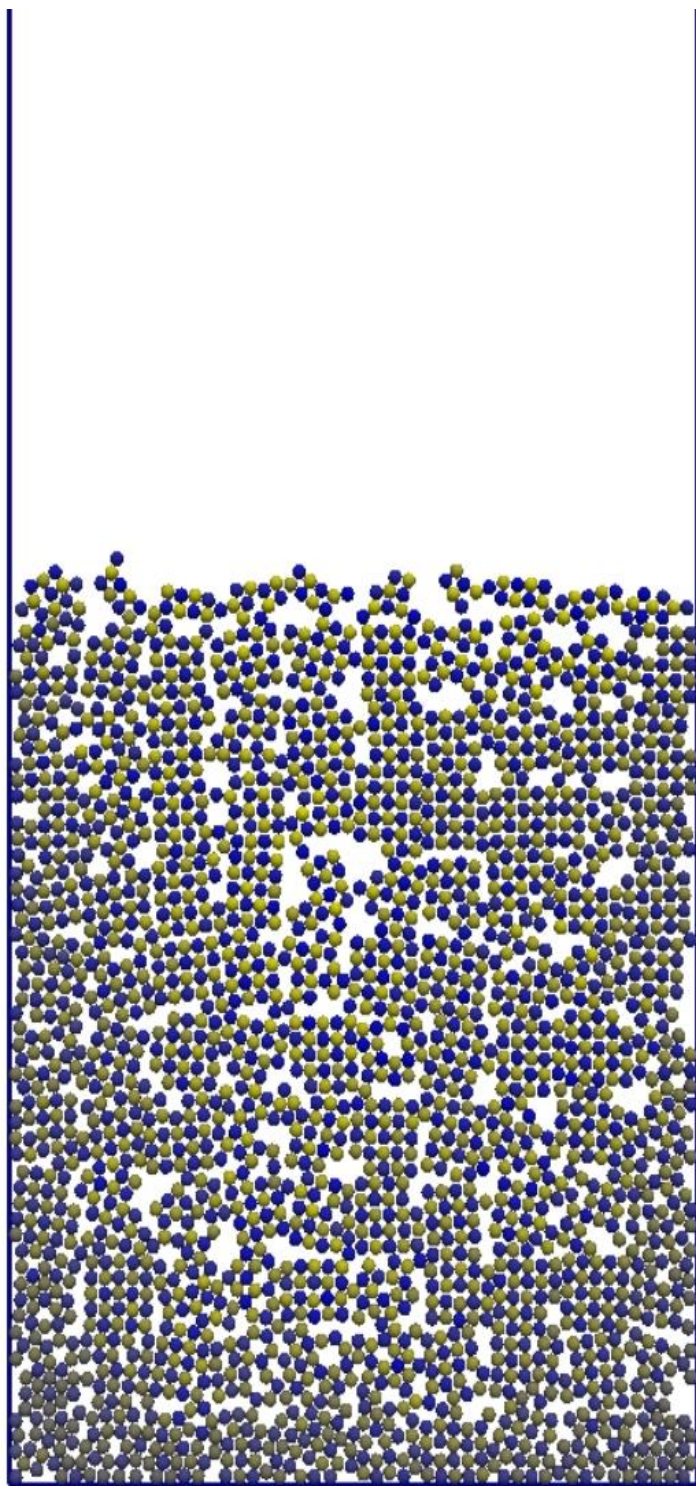
Figure 5c

(a) $v_g = 25$ mm·s^{-1}

Figure 6a
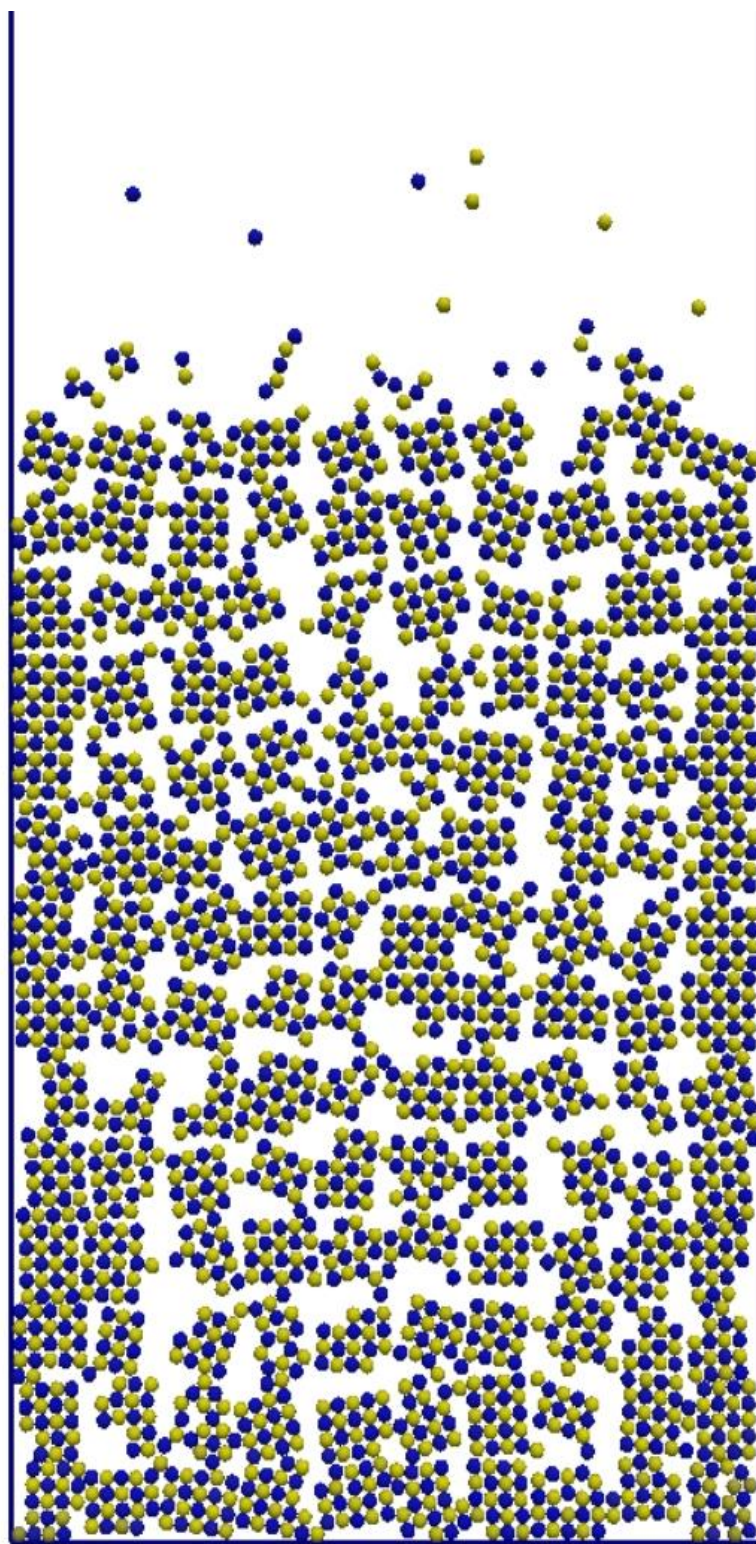
(b) $v_g = 50$ mm·s^{-1}

Figure 6b
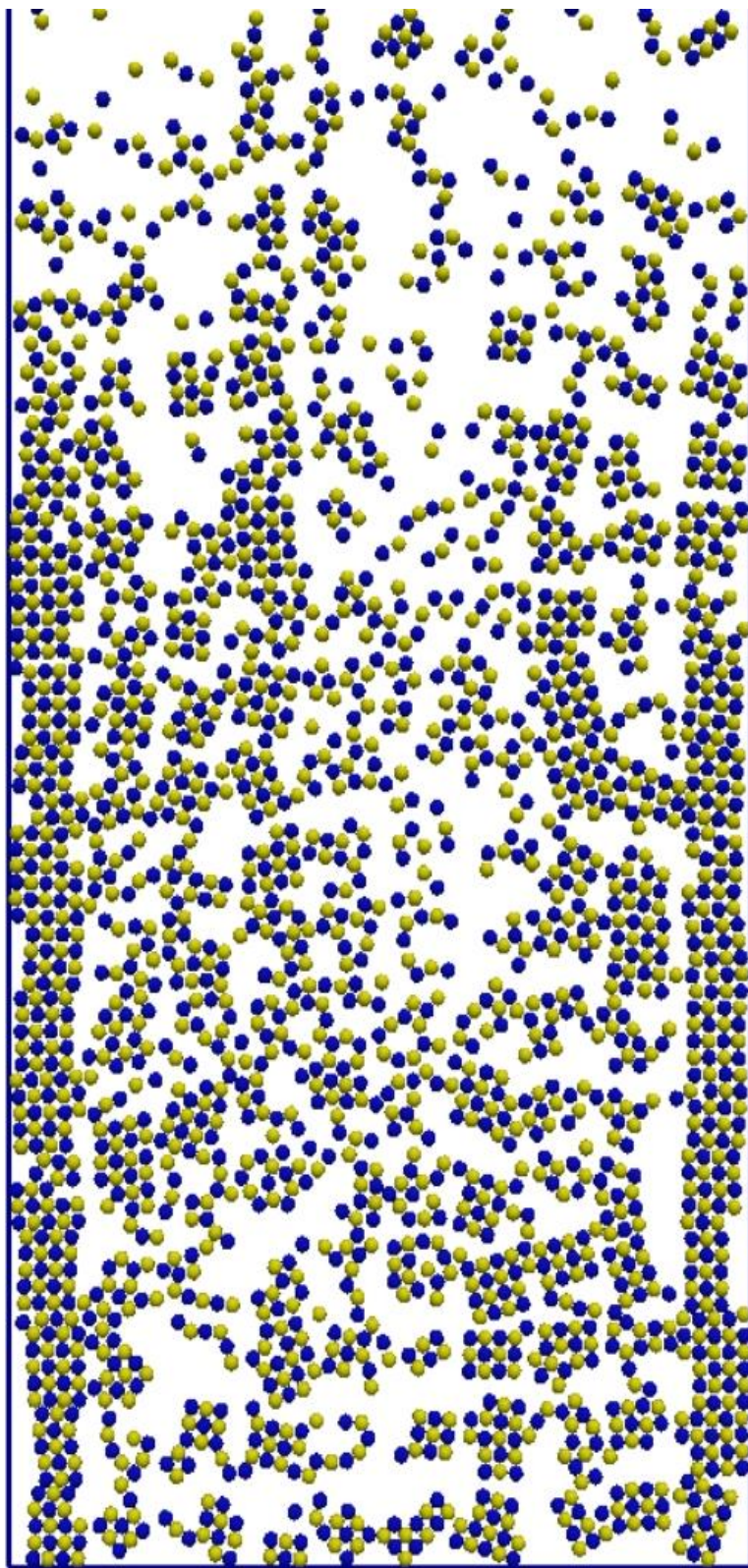
(c) $v_g = 100$ mm·s^{-1}

Figure 6c
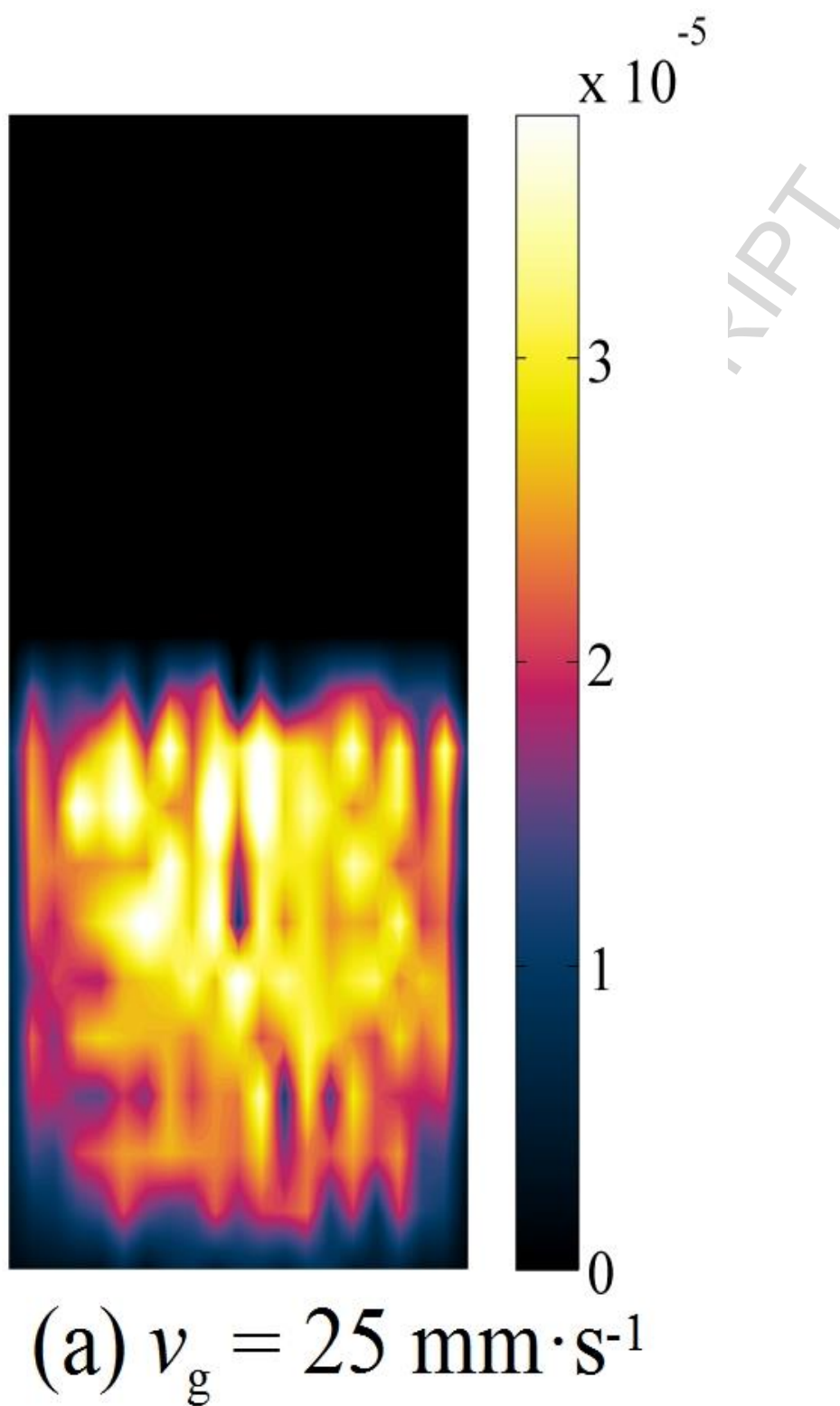
(a) $v_g = 25$ mm·s^{-1}
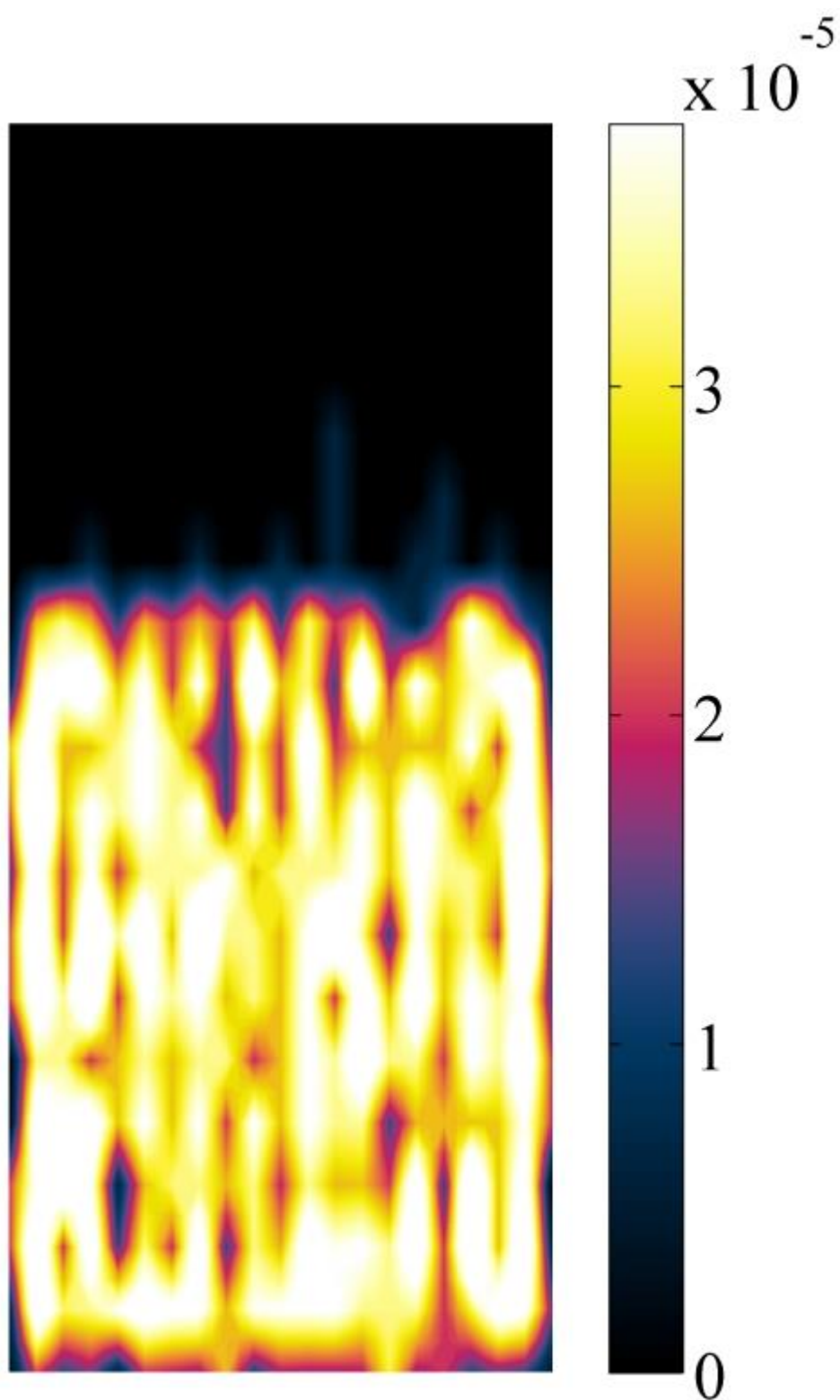
Figure 7a

(b) $v_g = 50$ mm·s^{-1}

Figure 7b
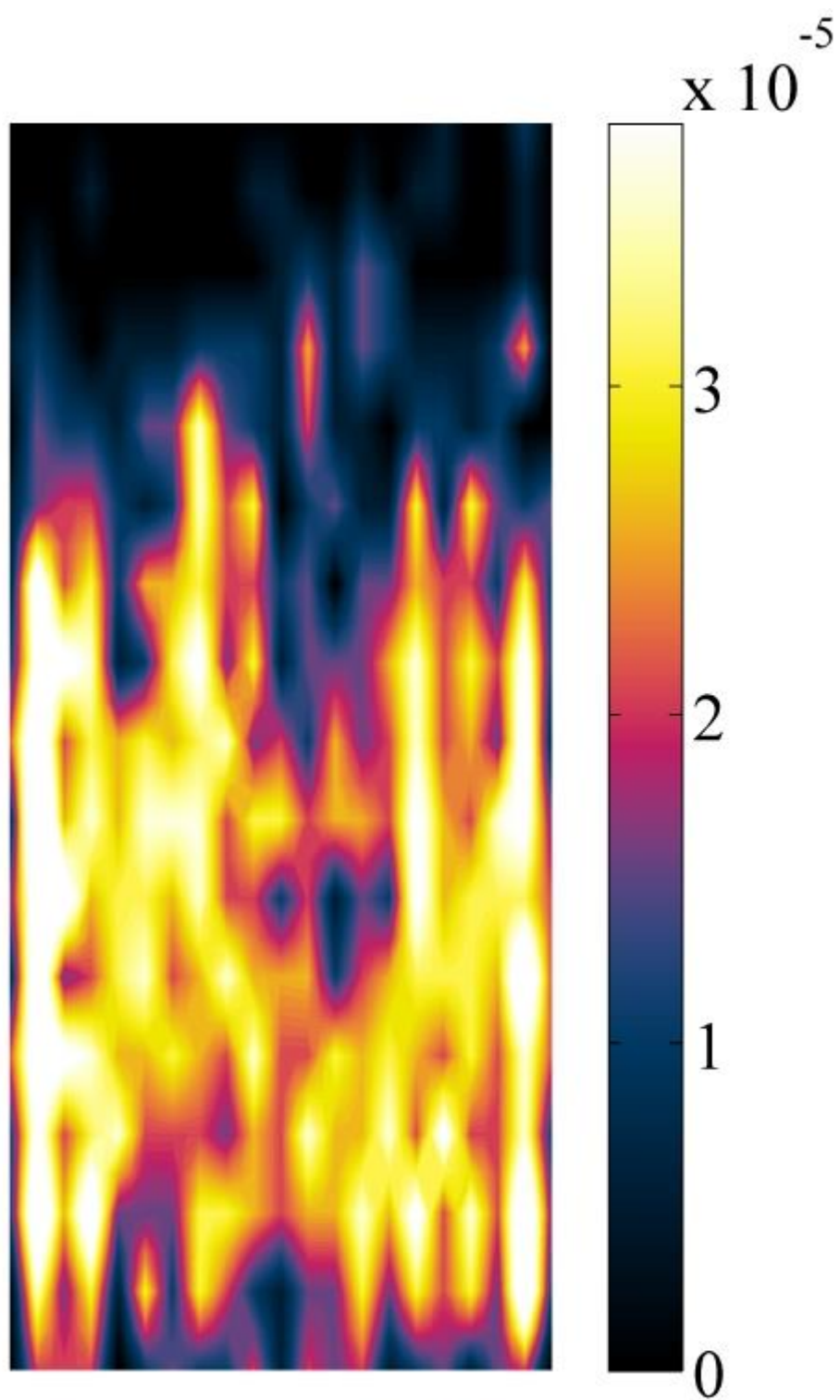
(c) $v_g = 100$ mm·s^{-1}

Figure 7c
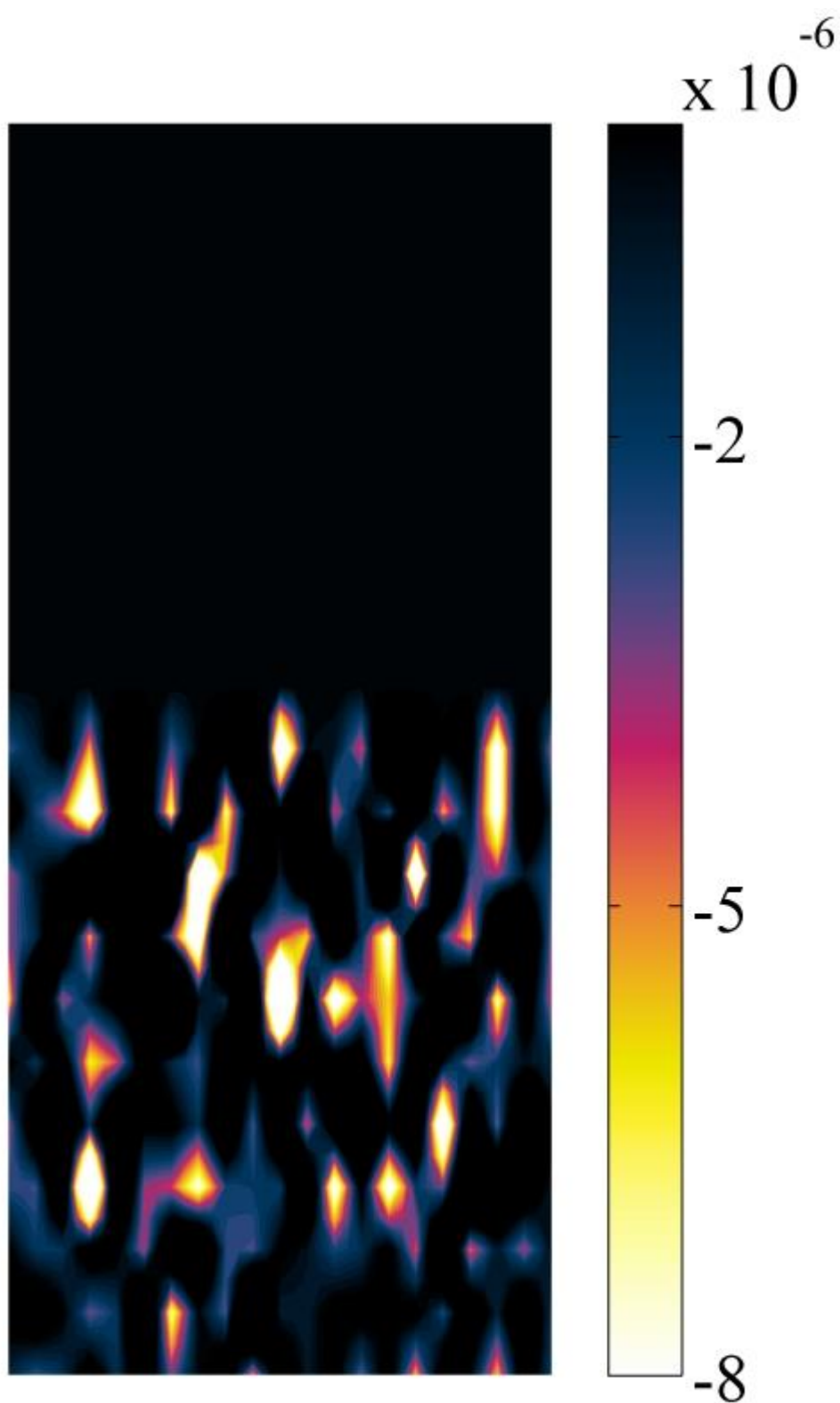
(a) $v_g = 25 \ mm \cdot s^{-1}$

Figure 8a
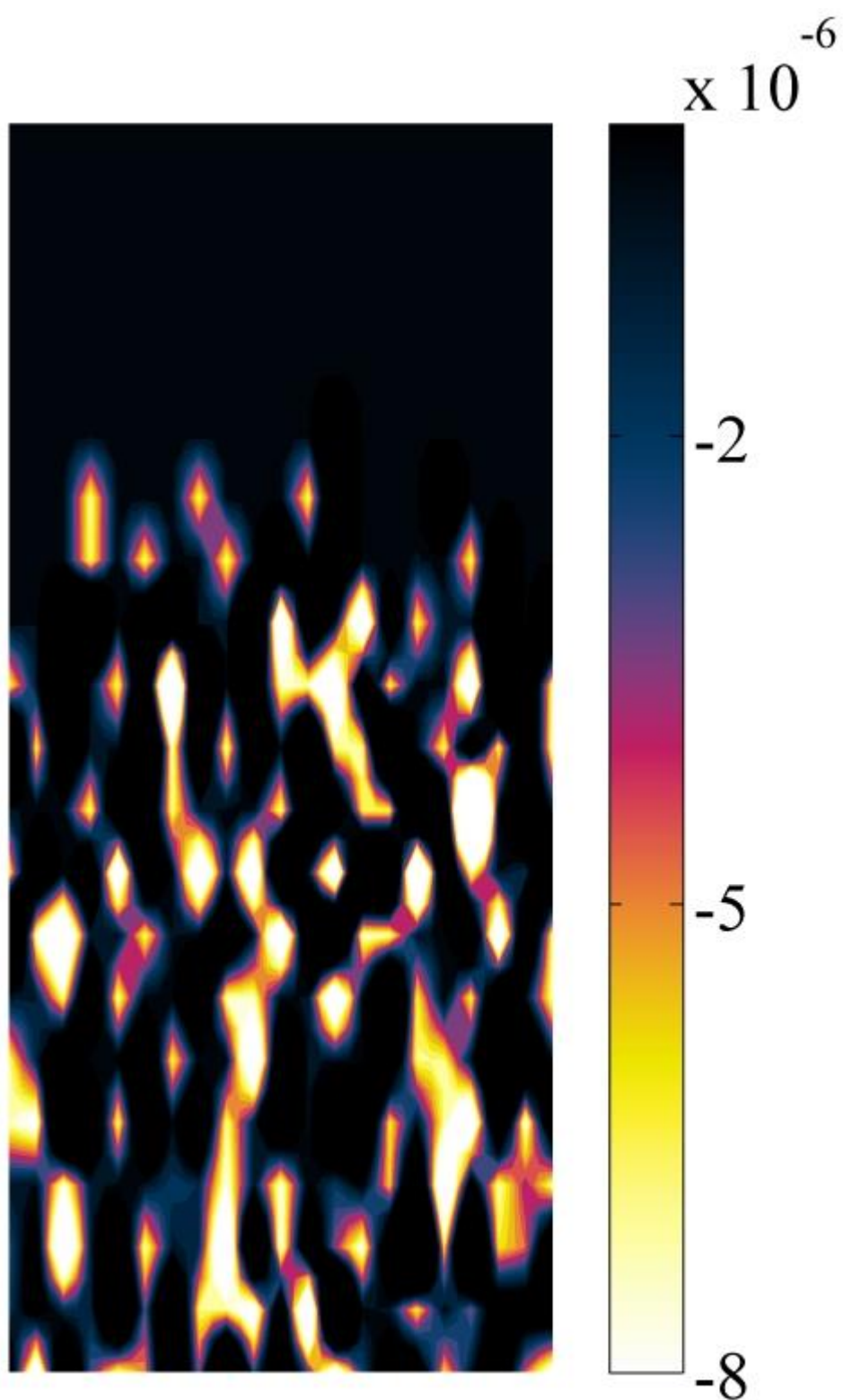
(b) $v_g = 50$ mm·s^{-1}

Figure 8b
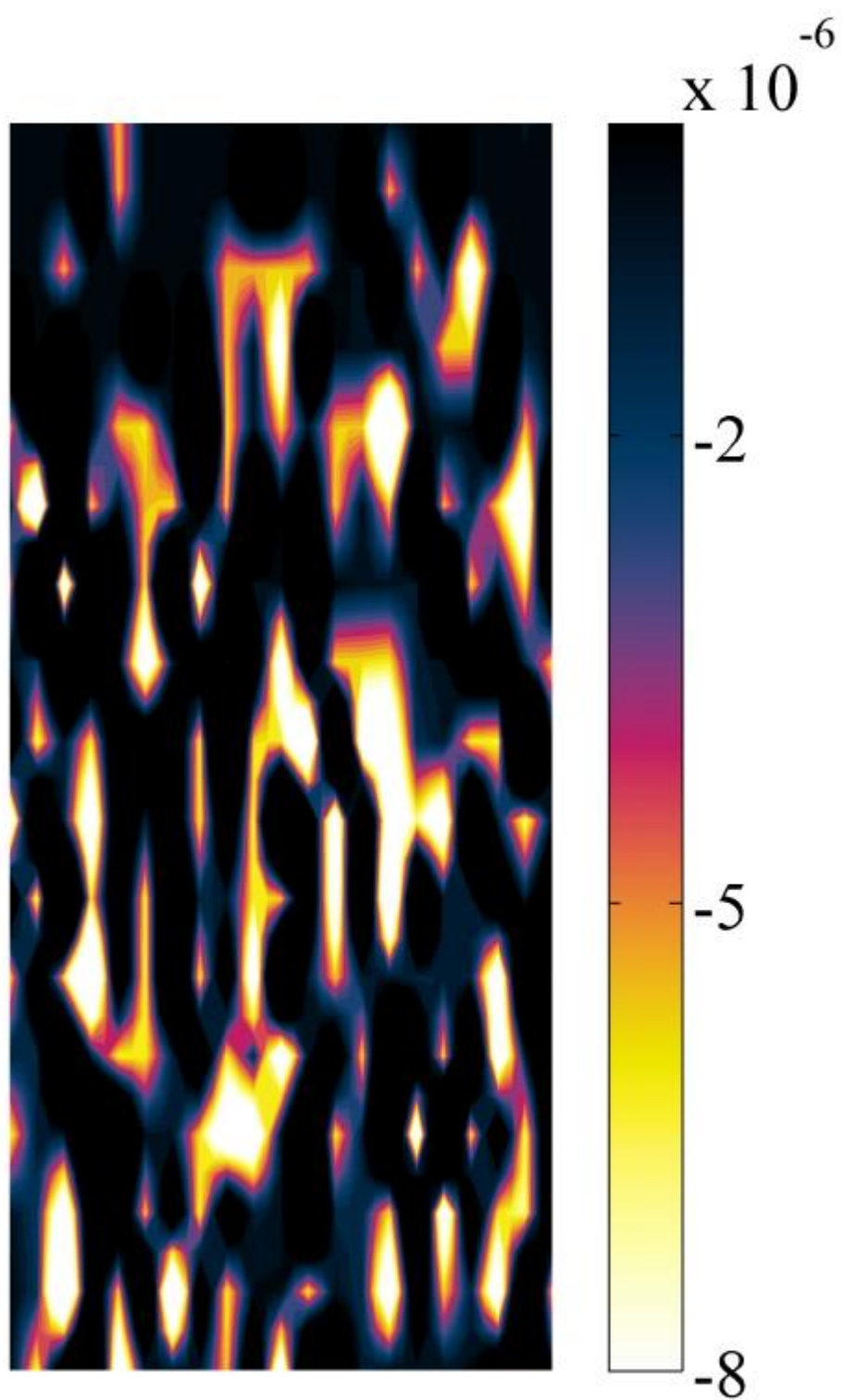
(c) $v_g = 100$ mm·s^{-1}

Figure 8c
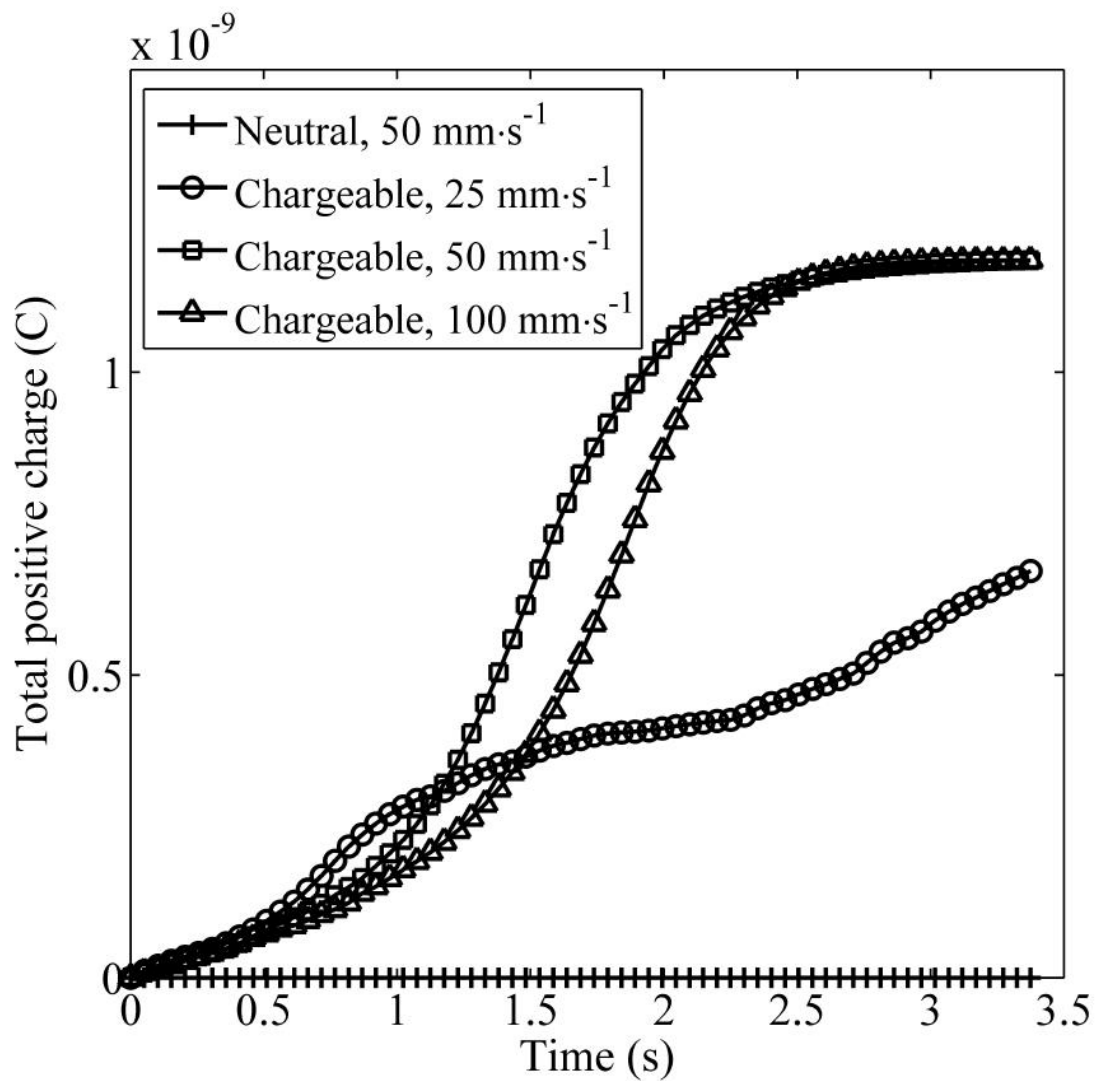
(a) Positive charge

Figure 9a
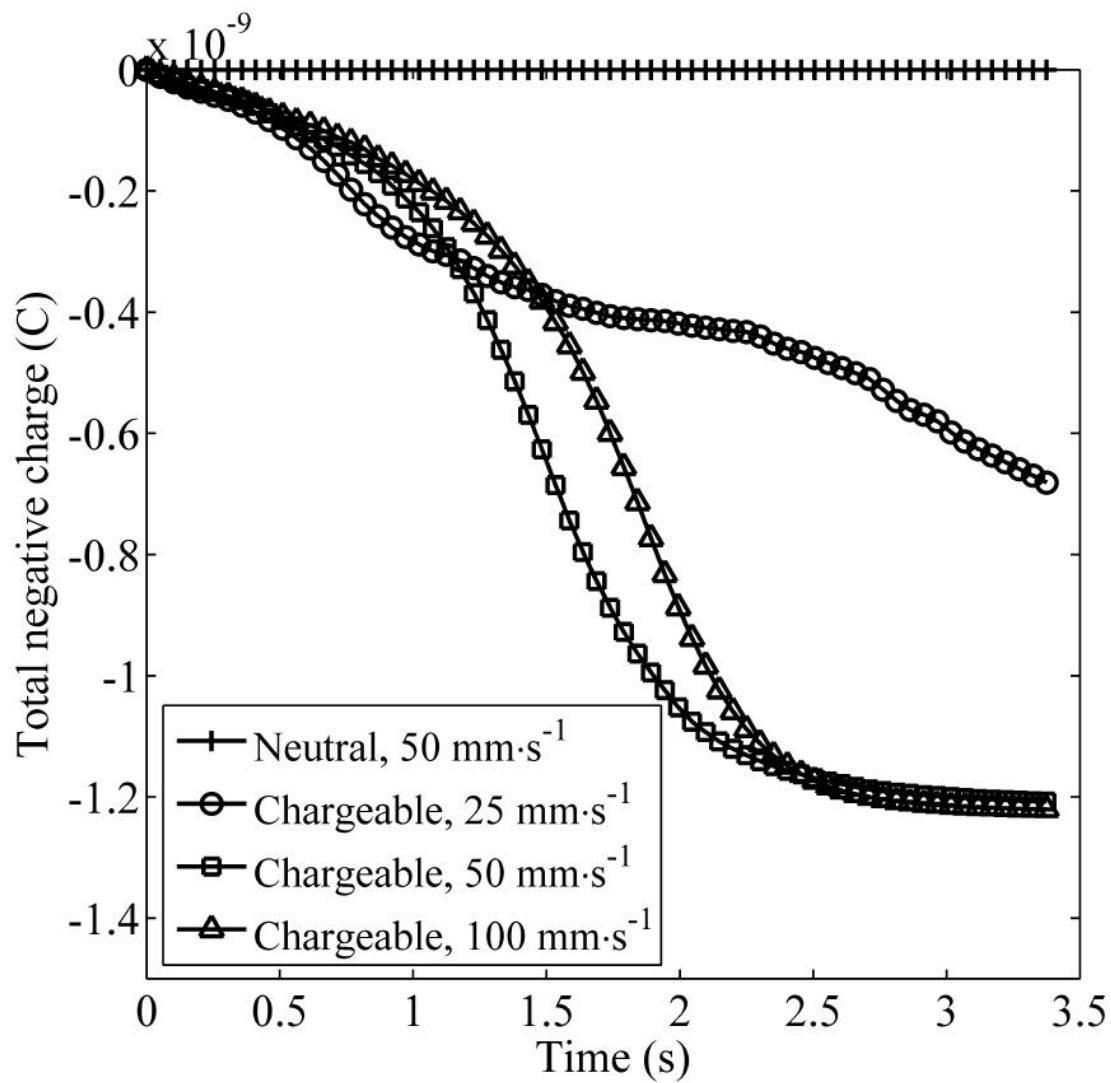
(b) Negative charge

Figure 9b
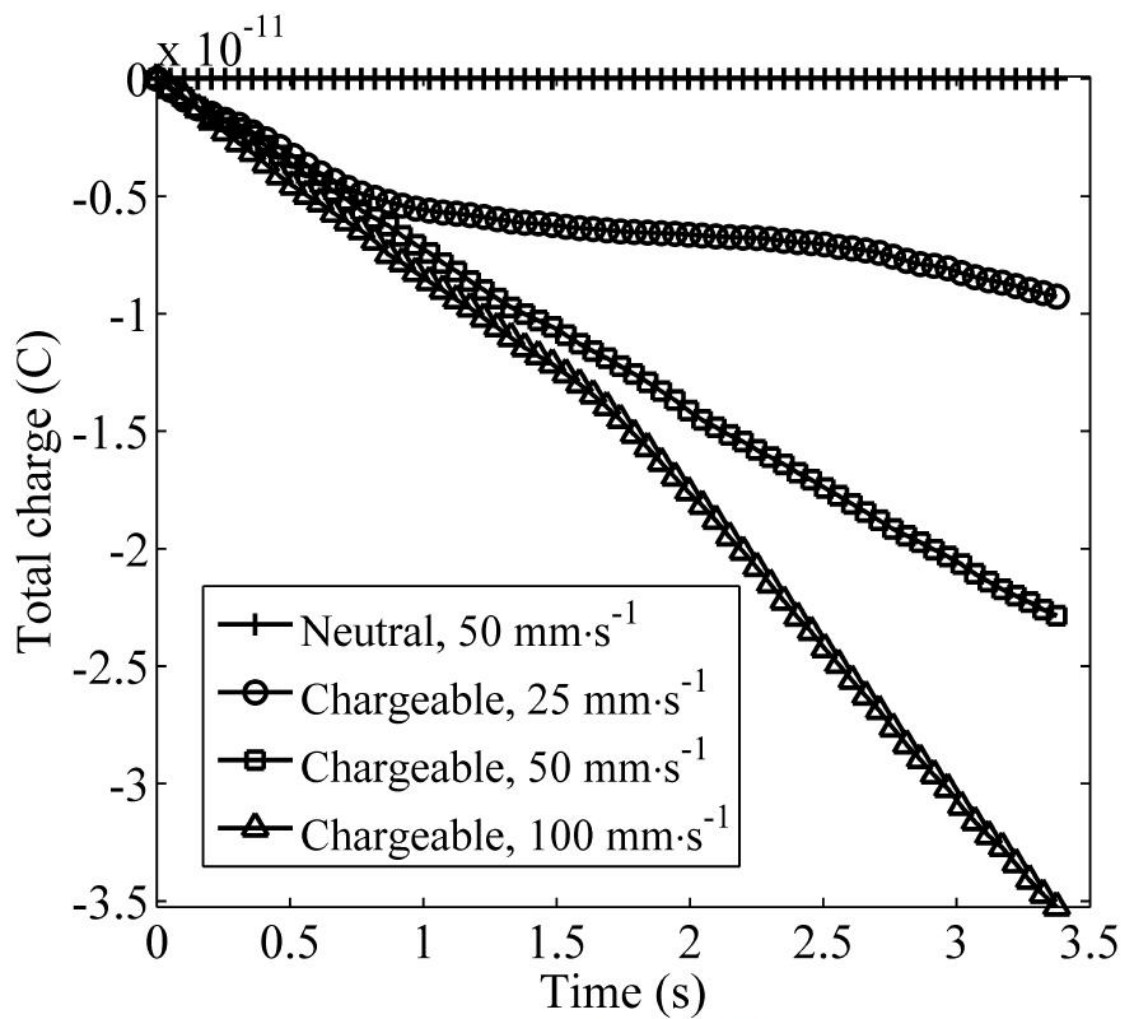
(c) Total net charge

Figure 9c
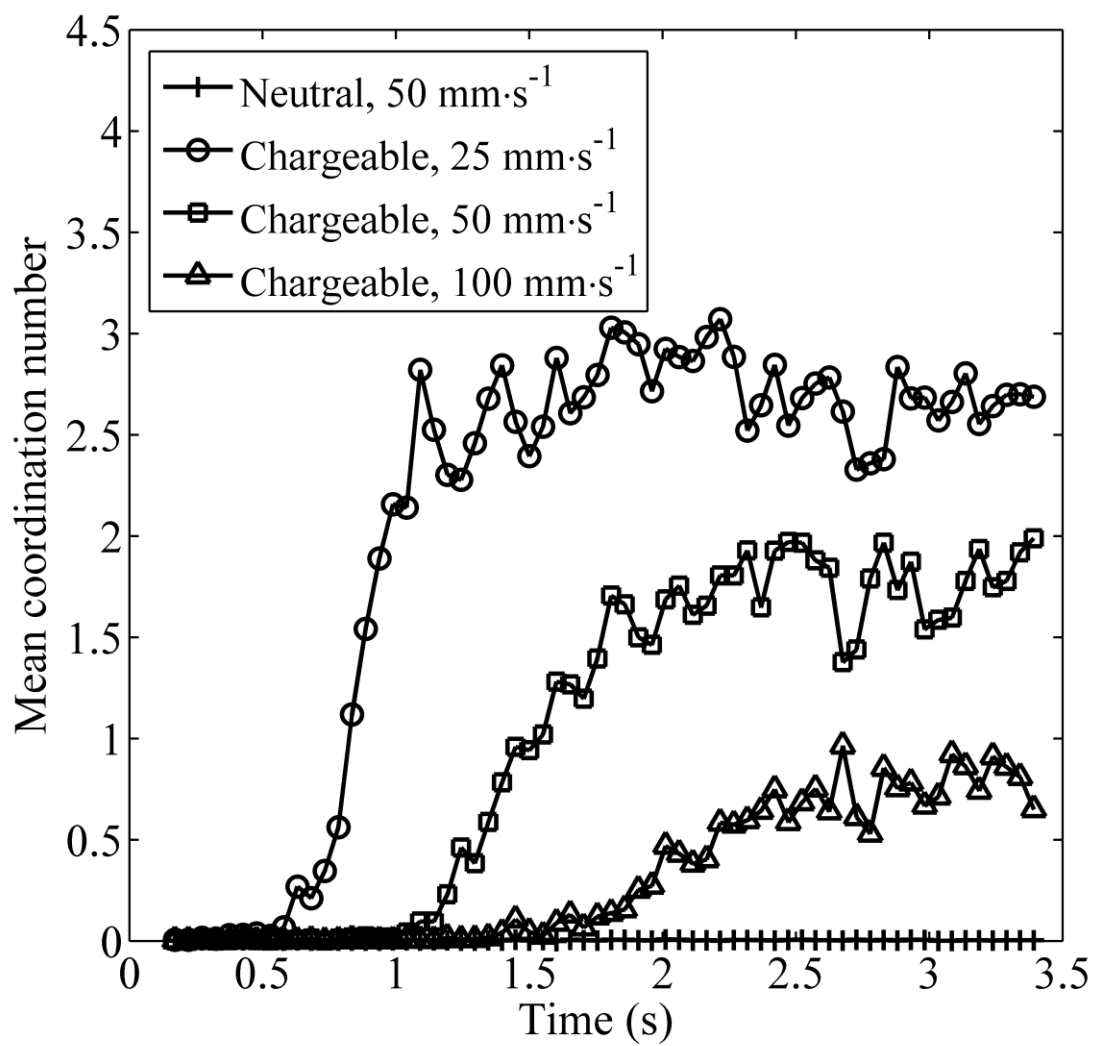
Figure 10
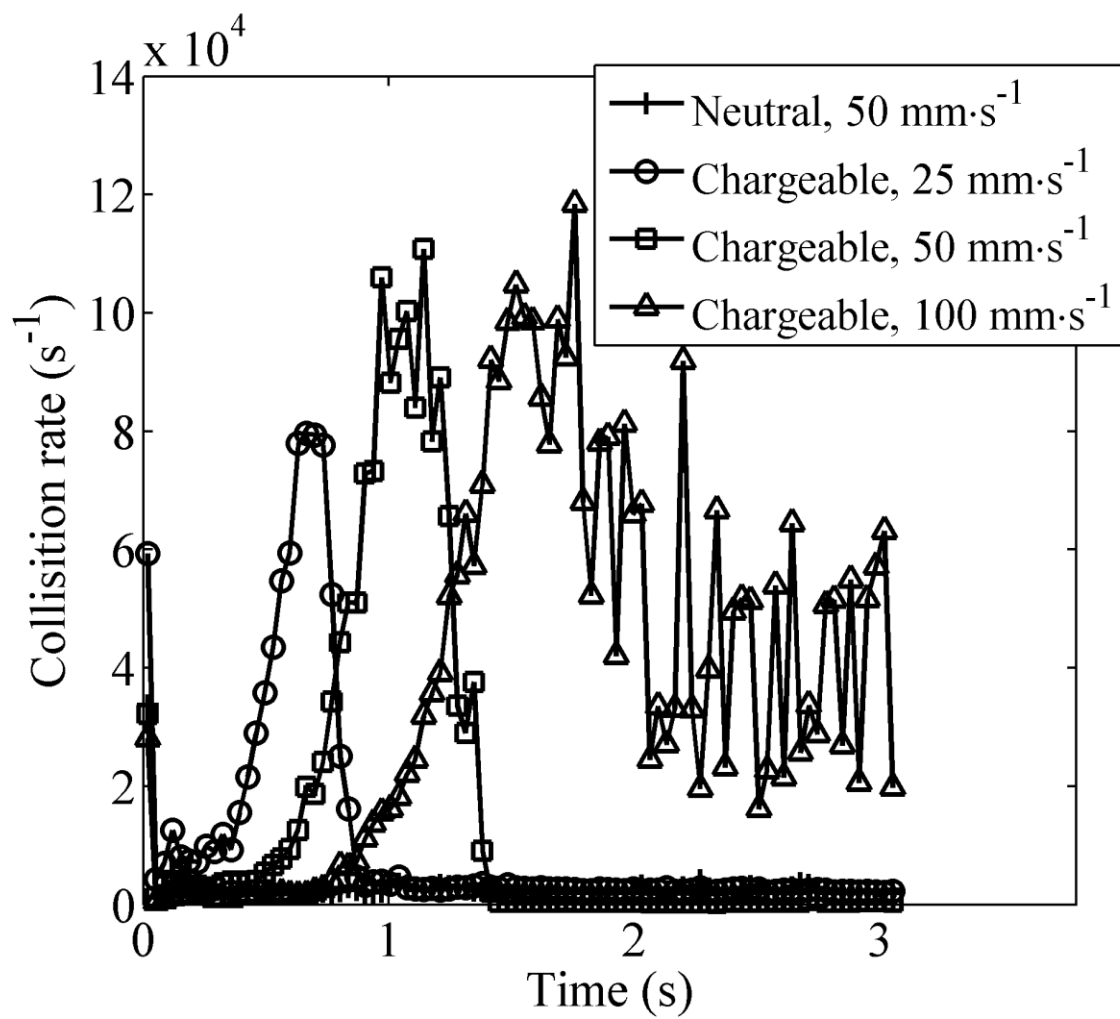
Figure 11
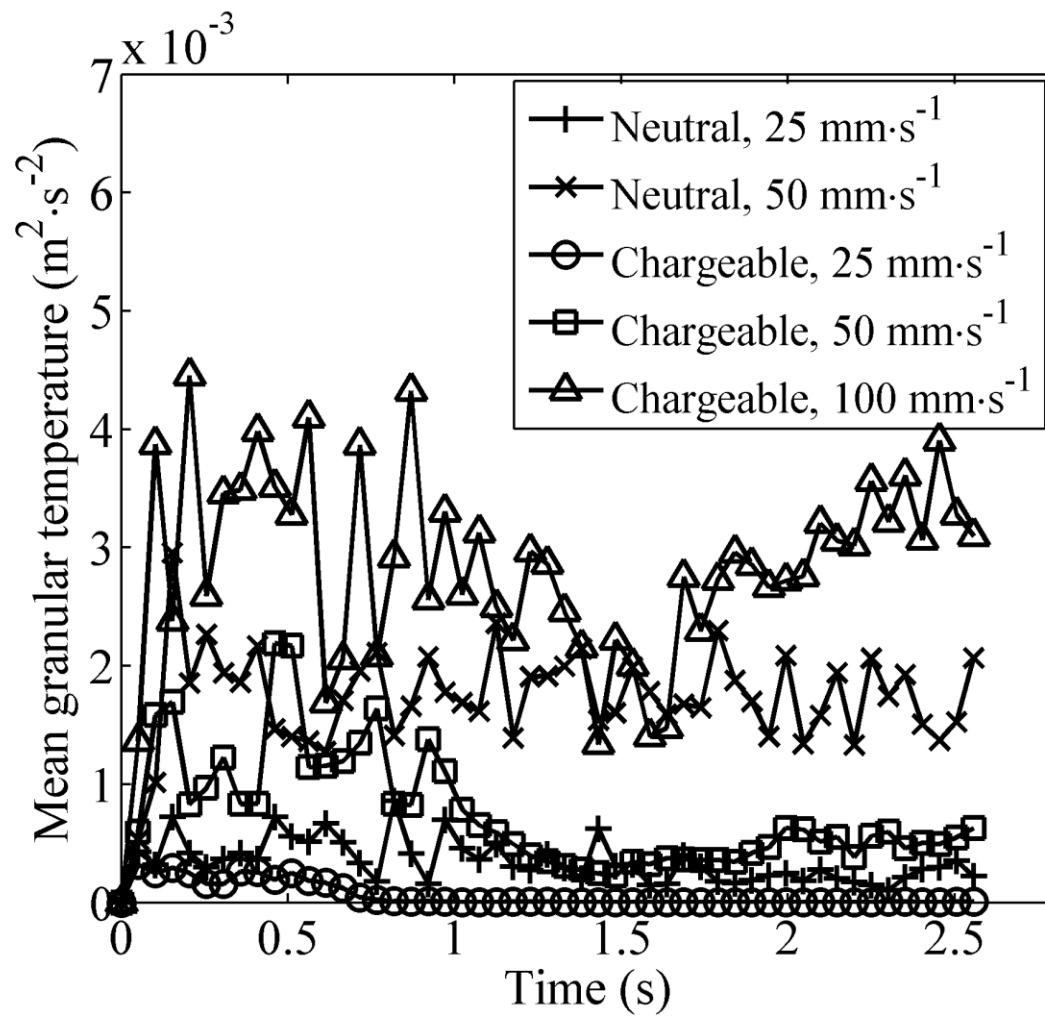
Figure 12
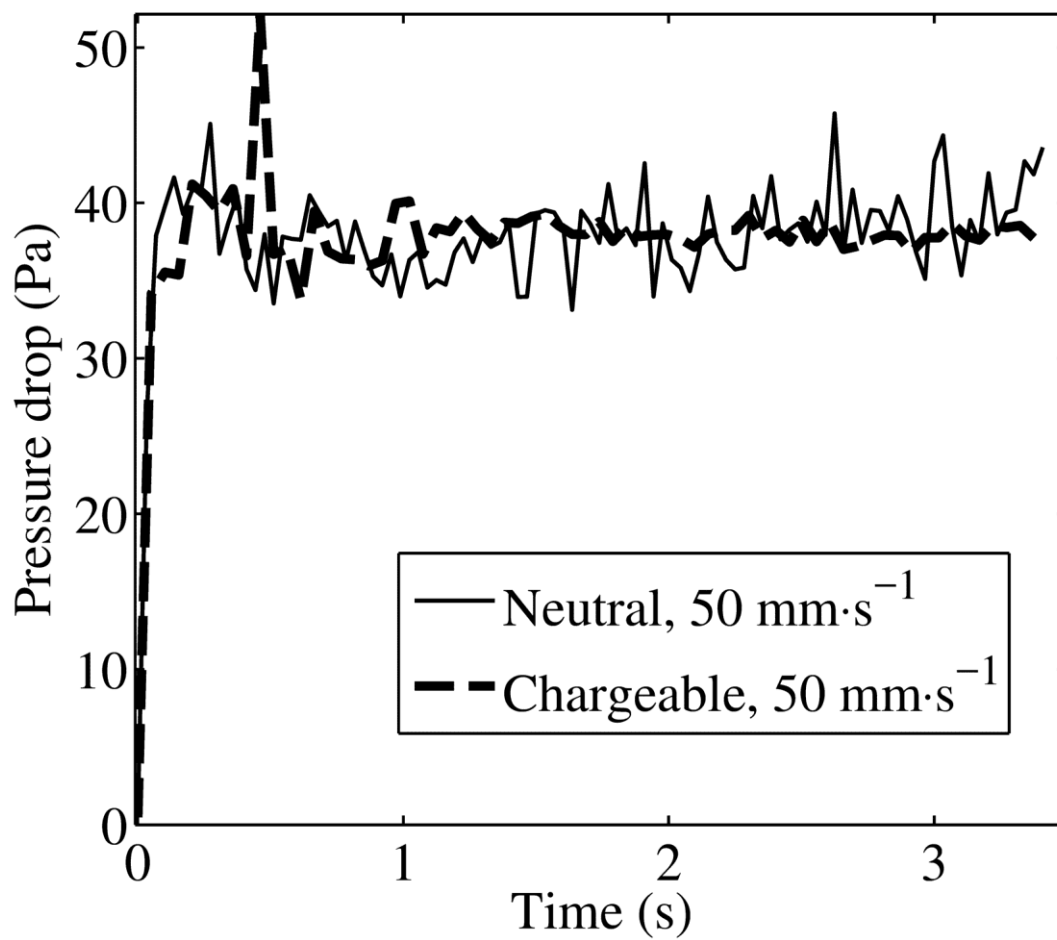
Figure 13
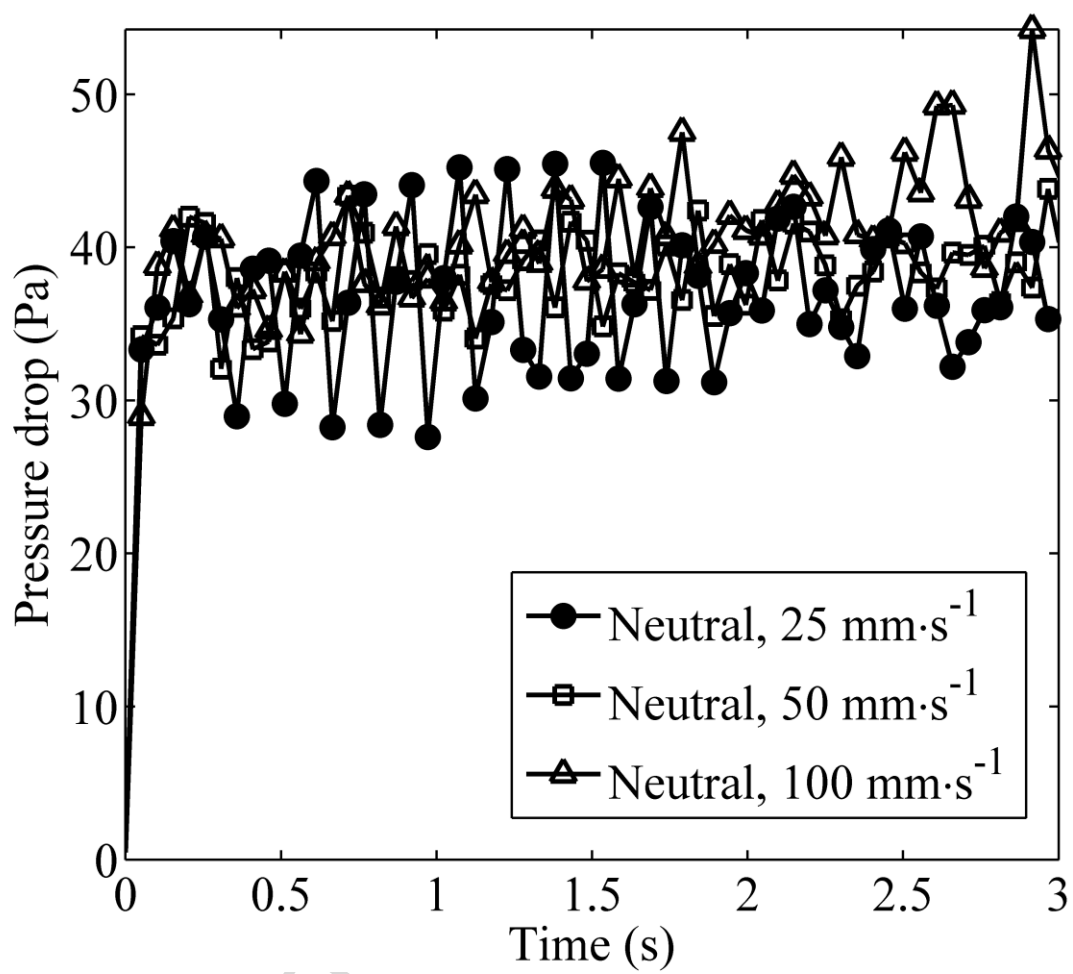
Figure 14

Figure 15

List of Figures

List of Tables

Table 1 Properties of the particle and the column

	Particle	Column
Young's module, Y (GPa),	8.9	210
Poisson's ratio, υ	0.3	0.3
Density, ρ (kg·m^{-3})	1500	7800

$v_g = 50$ mm·s^{-1} $v_g = 100$ mm·s^{-1}
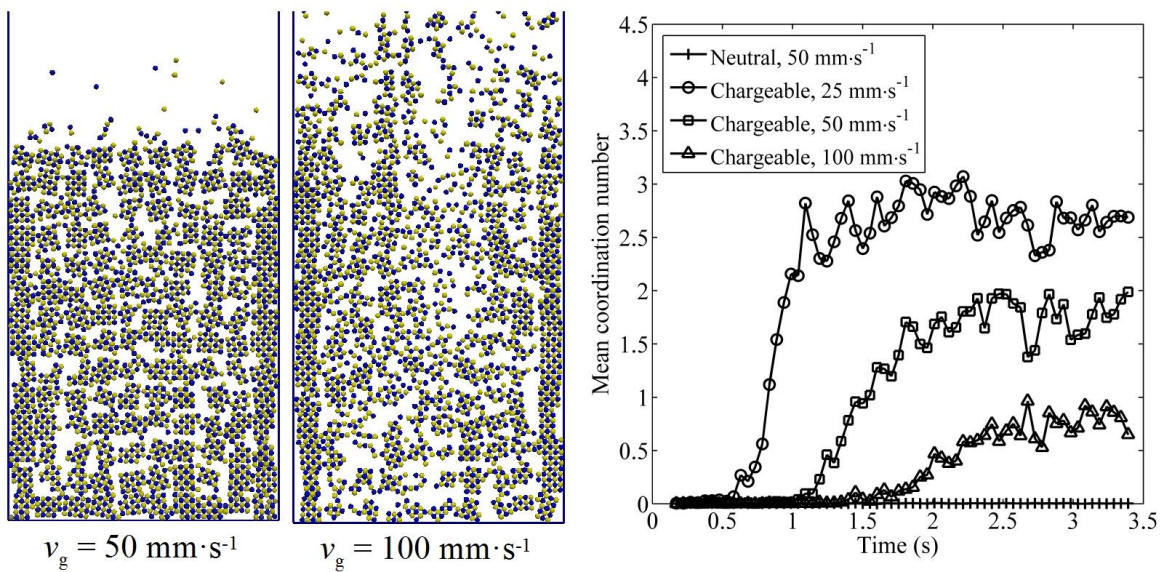
Graphical abstract

Highlights

- Contact electrification and electrostatic interactions are implemented into DEM-CFD
- Particles with different work functions are charged positively and negatively
- Bi-charged particles form agglomerates and affect the fluidization
- A high gas velocity can break agglomerates and leads to larger charge accumulation
- The agglomeration alters the pressure drop and increase the bubbling velocity